CHARACTERIZING THE RELATIVE TIMING AND CONDITIONS OF GOLD AND BASE-METAL DEPOSITION IN THE NORTHERN PART OF THE YELLOWKNIFE GREENSTONE BELT, NORTHWEST TERRITORIES, CANADA

A Thesis presented to the Faculty of the Graduate School at the University of Missouri-Columbia

---

In Partial Fulfillment of the Requirements for the Degree

Master of Science

---

by

AMANDA D. SMITH

Dr. Kevin L. Shelton, Thesis Supervisor

MAY 2011

The undersigned, appointed by the dean of the Graduate School, have examined the thesis entitled:

CHARACTERIZING THE RELATIVE TIMING AND CONDITIONS OF GOLD AND BASE-METAL DEPOSITION IN THE NORTHERN PART OF THE YELLOWKNIFE GREENSTONE BELT, NORTHWEST TERRITORIES, CANADA

Presented by Amanda D. Smith, a candidate for the degree of Master of Science

And hereby certify that, in their opinion, it is worthy of acceptance.

Kevin L. Shelton

Robert L. Bauer

Louis M. Ross. Jr.

ACKNOWLEDGEMENTS

This project would not have been possible without the guidance and contributions of my advisor, Kevin Shelton. I also thank Hendrik Falck of the Northwest Territories Geoscience Office for his invaluable knowledge and assistance in the field. I would like to thank Logan Hill for his help in the field and the lab. Lou Ross provided oversight and aid during SEM work at the University of Missouri. Dave Lovell of Yellowknife generously provided lodging in the field during summer 2009. Finally, I thank Dr. Kevin Shelton, Dr. Bob Bauer and Lou Ross who provided guidance with editing and finalizing this thesis and for serving on my thesis committee.

Financial support for this research was made possible by the Northwest Territories Geoscience Office, the Society of Economic Geologists Canada Foundation, the University of Missouri's MIDAS Ore Research and John and Betty Marshall Opportunities for Excellence funds.

TABLE OF CONTENTS

LIST OF FIGURES

LIST OF TABLES

CHARACTERIZING THE RELATIVE TIMING AND CONDITIONS OF GOLD AND BASE-METAL DEPOSITION IN THE NORTHERN PART OF THE YELLOWKNIFE GREENSTONE BELT, NORTHWEST TERRITORIES, CANADA

Amanda D. Smith

Dr. Kevin L. Shelton Thesis Supervisor

ABSTRACT

A complexity of gold-mineralization styles is recognized in the north end of the Yellowknife greenstone belt (YGB), ~30 km north of Yellowknife. These include volcanogenic massive sulfides, sulfide zones at intersections of shear zones, and quartz veins crosscutting metavolcanic and intrusive rocks. Gold-mineralized areas are hosted in the Kam Group and Banting Group metavolcanic and metasedimentary rocks, which are older and younger, respectively, than rocks that host major ore bodies in Yellowknife. Ore petrology of each group shows early arsenopyrite-pyrite-gold deposition followed by later base-metal sulfide overprinting. Mineralization in the Banting Group is dominated by abundant pyrrhotite, a feature not observed in the Kam Group. This may indicate that chemically unique ore-depositing systems operated within the Kam and Banting Groups. Fluid inclusion, cathodoluminescence and stable isotope studies allow documentation of the nature of multiple fluids that affected these rocks.

Dolomite-ankerite in quartz veins of the Kam Group exhibits similar cathodoluminescence zoning (CL) in mineral showings up to 5 km apart. Similar

CL zoning is not observed in carbonates in the Banting Group. However, paragenetically later calcite exhibits similar CL patterns in both stratigraphic groups.

Four types of fluid inclusions in the Kam Group showings have been identified. H_2O-CO_2 inclusions were found in relatively undeformed quartz grains and have T_h values of 316° to 394°C. These rare inclusions are thought to represent ore fluids penecontemporaneous with regional metamorphism of the host rocks. These fluids are similar to primary ore fluids found in other greenstone-hosted gold deposits. Carbonic (CO_2±CH_4) inclusions likely formed by subsequent modification of H_2O-CO_2 inclusions. Halite-bearing and aqueous brine inclusions are ubiquitous in the Kam and Banting Groups, in both mineralized and barren quartz veins. T_h values for these inclusions are dominantly 110° to 260°C, with a minor higher temperature population >270°C. These aqueous brines are similar to those observed in quartz veins in the Proterozoic West Bay Fault to the south and likely represent brine movement associated with reactivation of similar faults.

Quartz veins in mineralized metavolcanic rocks of Chan Lake, Greyling Lake, Homer Lake, and Oro Lake (Kam Group) have $\delta^{18}O$ values from 9.9 to 11.8‰ V-SMOW (n=16) deposited from fluids with $\delta^{18}O_{water}$ values of 4.1 to 7.2‰. Quartz veins from Banting Group rocks (Kingfisher Island, Ann claims, Banting Lake and Samex Island) have $\delta^{18}O$ values of 13.2 to 14.9‰ (n=5) and were deposited from fluids with $\delta^{18}O_{water}$ values of 7.4 to 10.3‰, reflecting the influence of metasedimentary rocks in this group. Similar influences of both

metavolcanic and metasedimentary fluid sources were documented in previous studies of the world-class Giant mine.

Data are interpreted to indicate that distinct styles of gold mineralization in the Kam and Banting Groups formed from their own individual hydrothermal systems. Post-ore, dolomite-ankerite-depositing fluids indicate a continuity of fluid circulation through the Kam Group, but a lack of fluid communication between the Kam and Banting Groups. Later fluids, evidenced by calcite CL and aqueous brine inclusions, moved ubiquitously throughout both groups.

CHARACTERIZING THE RELATIVE TIMING AND CONDITIONS OF GOLD AND BASE-METAL DEPOSITION IN THE NORTHERN PART OF THE YELLOWKNIFE GREENSTONE BELT, NORTHWEST TERRITORIES, CANADA

CHAPTER I: INTRODUCTION

Mineral exploration and mining have been important aspects of the economy for Yellowknife, Northwest Territories for more than sixty years. The Northwest Territories is known historically for numerous geological resources, including gold deposits, natural gas, and diamondiferous kimberlite pipes. The Yellowknife greenstone belt of the Northwest Territories is host to the world-class Giant, Con, and Discovery gold mines, which collectively yielded some 13.5 million ounces of gold since active mining initiated at the Con Mine in 1938 (Bullen and Robb, 2006).

Much of economic mineral development in the Yellowknife greenstone belt (YGB) has shifted to kimberlite exploration due to the closure of the Giant and Con mines in the early 2000's. Currently, there are only a few active regions with exploration projects seeking gold, but one of the more promising regions is the north end of the Yellowknife greenstone belt, approximately 30 to 100 km north of Yellowknife (Fig. 1). Numerous showings have been discovered within and adjacent to the volcanic rocks making up the YGB, but discovery of a major concentration of gold has been elusive.

A complexity of gold-mineralization styles is recognized in the north end of the Yellowknife greenstone belt. These gold-mineralized areas are hosted in Kam Group (Chan Formation) and Banting Group metavolcanic and metasedimentary rocks, which are older and younger, respectively, than those that host the Con and Giant mines in Yellowknife. Previous work (Kerswill and Falck, 2002) has shown that the north end of the YGB contains gold showings with characteristics different from the classic shear-zone hosted gold deposits in Yellowknife (Giant and Con Mines). The north end deserves further investigation to understand the development of these disparate gold-rich areas and their relationship to gold-bearing hydrothermal systems that were present elsewhere in the YGB. This study describes the paragenesis, geochemistry, and relative timing of gold and base metal-emplacement in the north end of the YGB through combined applications of ore petrology, cathodoluminescence studies, fluid inclusion microthermometry, and oxygen isotope geochemistry.

Specific questions addressed in this study include: (1) What is the fluid history of gold and base-metal sulfide mineralization in the Kam and Banting Groups of the north end of the YGB? (2) In particular, what are the P-T-X conditions of the ore-bearing and post-ore fluids? (3) What are the ore mineralogy and paragenesis at each locality and how do they relate to potential metal and fluid sources? (4) What can this tell us about fluid flow within and between the Kam and Banting Groups?

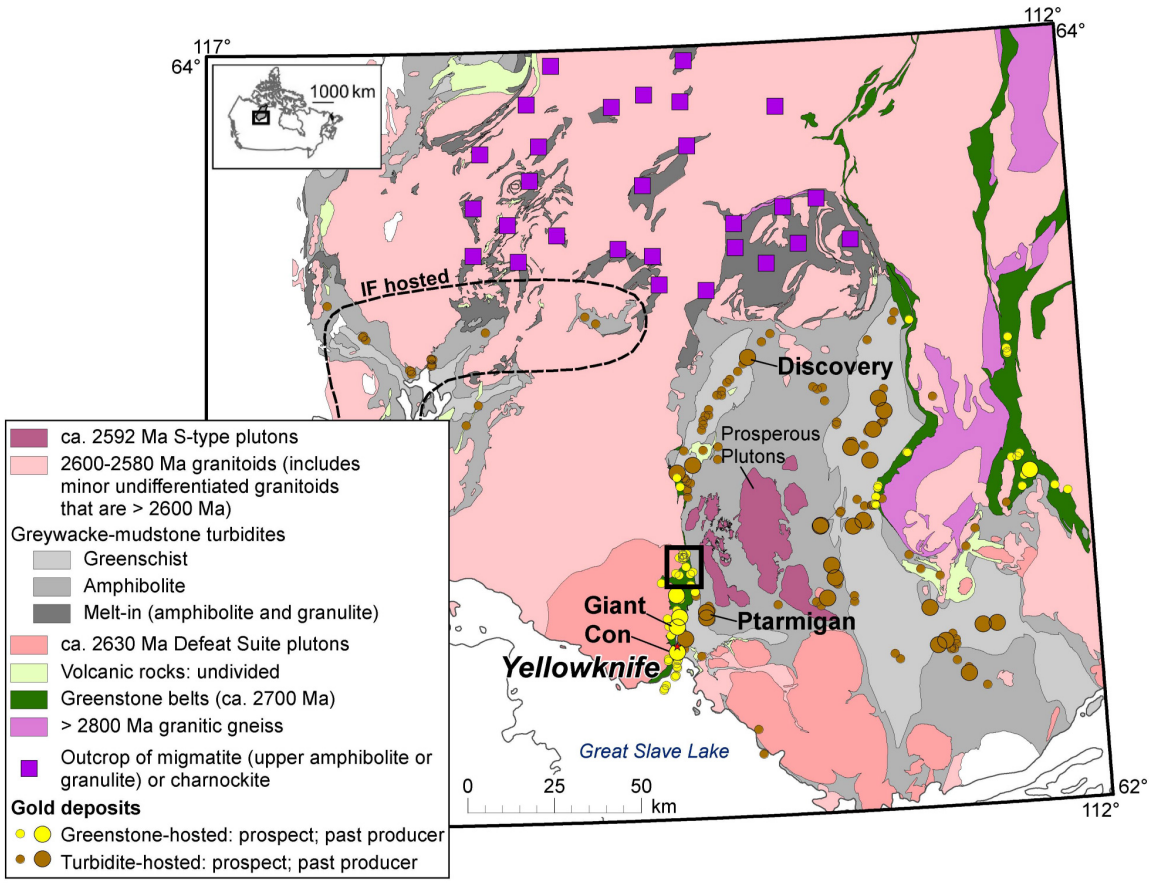

Figure 1. General geology of the Yellowknife greenstone belt; the black box outlines the approximate study area hosted in the Kam and Banting Groups; IF=iron formation-hosted deposits (Modified after Ootes et al., 2011).

GEOLOGIC BACKGROUND

This research focuses on gold and base-metal mineralized areas hosted in Archean metavolcanic and metasedimentary rocks of the Kam Group (Chan Formation) and Banting Group in the north end of the Yellowknife greenstone belt (YGB), approximately 30 km north of Yellowknife.

Field observations of showings hosted in the Chan Formation (Kam Group) and Banting Group of the YGB confirm a complexity of mineralization styles, including volcanogenic massive sulfide (VMS) type mineralization, and accumulations of gold and base-metal sulfides in shear zones.

Slave Craton

Located in the Northwest Territories in northern Canada, the Archean Slave craton is one of the most distinct and exotic building blocks of North America and is a major component of the Canadian Shield. The Slave craton is one of thirty-five Archean crustal provinces that are recognized worldwide and is a relatively small craton, approximately 210,000 km^2, bounded in the south, east, and west by Paleoproterozoic orogenic belts (Davis et al., 2003). The Slave craton is comprised of an Archean gneissic basement overlain by a Archean supracrustal assemblage (ca. 2800-2600 Ma; Bleeker, 2002) and is intruded by several Archean plutons (ca. 2700, 2760, 2635-2620, and 2610-2602 Ma; van Breeman et al., 1992; Davis and Bleeker, 1999, Pehrsson and Villeneuve, 1999: Ketchum et al., 2004; Bennett et al., 2005; Ootes et al., 2005, 2007; Bleeker and Hall. 2007). Plutonism in the Slave craton concluded in an extensive granite

bloom accompanied by widespread, regional metamorphism (2600-2500 Ma; Kusky, 1993; Davis and Bleeker, 1999), followed by cooling of the lower crust over a period of seventy million years (Bleeker and Hall, 2007).

Yellowknife Greenstone Belt

While the Slave craton is host to several greenstone belts, economic gold concentrations are found primarily within the craton's Yellowknife greenstone belt (YGB). The YGB (Fig. 1) is located in the southwestern part of the Slave Craton and is bounded by the Western Plutonic Complex to the west and metaturbiditic rocks of the Burwash Formation to the east (Bleeker and Hall, 2007). The belt extends approximately N-S for 100 km and hosts a succession of mafic to felsic metavolcanic rocks with minor meta-volcaniclastic and metsedimentary rocks. The metamorphic grade of the YGB ranges from greenschist to lower amphibolite facies within the metamorphosed mafic rocks (Bethune et al., 1999; Davis and Bleeker, 1999; MacLachlan and Davis, 2002; Thompson, 2006). Characteristic mineral assemblages in the YGB are albite-chlorite-actinolite-epidote (greenschist zone), calcic plagioclase-actinolite-hornblende-epidote/chlorite (transitional zone), and hornblende-calcic plagioclase (amphibolite zone; Thompson, 2002).

Major groups of the YGB, from older to younger, include: the Central Slave Basement Complex; the Central Slave Cover Group; the Kam Group; the Banting Group; metaturbidites of the Burwash and Walsh Formations of the Duncan Lake Group; and metaconglomerates of the Jackson Lake Formation.

This research concentrates on the Archean metavolcanic and metasedimentary rocks of the Kam Group (Chan Formation) and Banting Group of the YGB.

Kam Group Geology

The Kam Group (Fig. 2) is approximately 10 km thick and is dominated by metamorphosed mafic pillow lavas with inclusions of original thin rhyolite tuffs, banded iron formation horizons, and komatiite flows (Bleeker and Hall, 2007). While portions of this sequence have been dated at 2722±1 and 2697±2 Ma (Isachsen and Bowring, 1997; Bleeker and Hall, 2007), a mafic dike that crosscuts the basal Chan Formation at Homer Lake (Fig. 4) yielded an age of 2738±2 Ma, indicating that there are older portions of group than previously known (J. Ketchum, pers. comm. *in* Bleeker and Hall, 2007). The Kam Group is divided into four formations from oldest to youngest: Chan Formation, Crestaurum Formation, Townsite Formation, and Yellowknife Bay Formation.

The basal Chan Formation of the Kam Group disconformably overlies the Central Slave Cover Group and is characterized by greenschist to amphibolite grade pillowed and massive thoeliitic basalts. The Chan Formation is of particular interest to this research due to the presence of multiple mineralization styles within a relatively small area.

Banting Group Geology

Between ~2.70 and 2.66 Ga, widespread volcanism was present throughout the Slave Craton (Davis et al., 2003). This calc-alkaline volcanism

was accompanied by rifting, and is supported by the presence of abundant metamorphosed felsic and intermediate rocks, tholeiitic to calc-alkaline basaltic rocks, and intercalated volcaniclastic sedimentary rocks (Bleeker and Hall, 2007). These rocks are classified as the Banting Group (Fig. 2, ca. 2.69 to 2.66 Ga) and are also referred to as the Hackett-type rocks (Kusky, 1989; Bleeker and Hall, 2007). These arc-like volcanic rocks of the Banting Group are absent in the western part of the Slave Craton and tend to dominate the eastern part (Ootes, 2004).

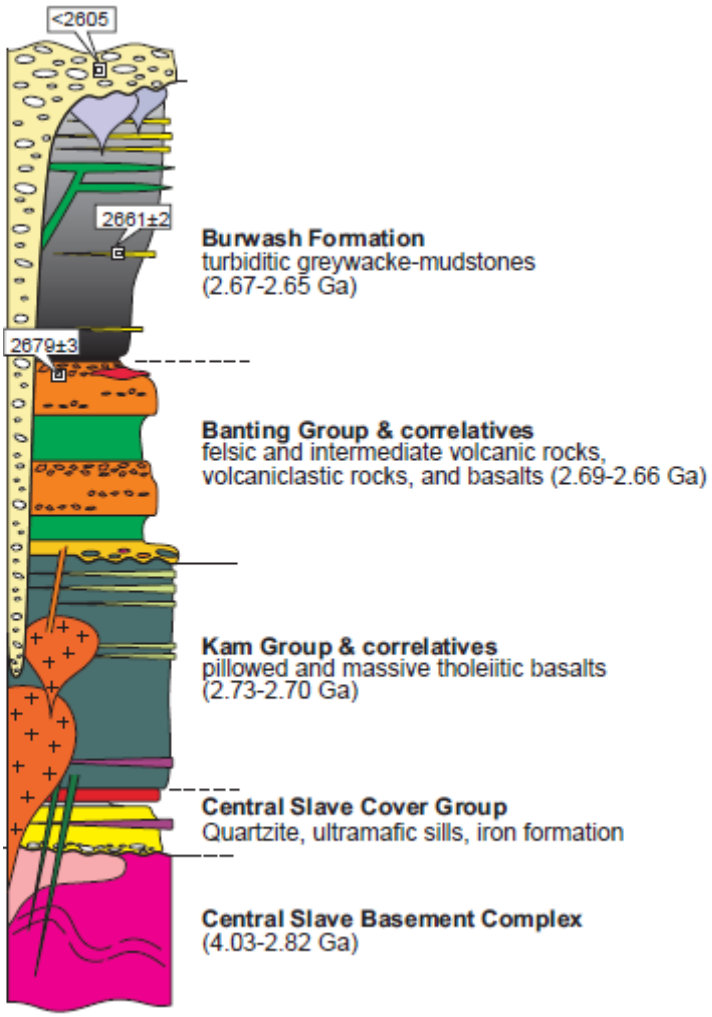

Figure 2: Stratigraphic column of Yellowknife Greenstone Belt (modified after Bleeker and Hall, 2007)

Metamorphism and Deformation in the Yellowknife Greenstone Belt

Multiple periods of metamorphism and deformation have been recognized in the Yellowknife greenstone belt and are constrained within the supracrustal rocks of the YGB by pre-, syn-, and post-deformational rocks (e.g. pluton emplacement; Davis and Bleeker, 1999; Bleeker, 2002; Ootes et al., 2005). Deformational features vary based on host rock lithology and proximity to the Yellowknife River Fault Zone (Fig. 3), which trends approximately N-S and defines the contact between the Kam and Banting Groups (Martel and Lin, 2006).

There are two major metamorphic events (M1 and M2) recognized in the YGB, in addition to several localized contact metamorphic events. The M1 event is related to contact metamorphism associated with intrusion of the Defeat Suite plutons of the Western Plutonic Complex (ca. 2.63-2.62 Ma; Bethune et al., 1999; Davis and Bleeker, 1999; MacLachlan and Davis, 2002; Thompson, 2006).

Following M1 metamorphism, overthickening of the crust due to regional shortening (D2) resulted in high temperature-low pressure (M2) metamorphism (Thompson, 2002). This regional metamorphic event transferred a significant portion of heat and lower crustal fluids to the upper crust. During this regional metamorphism, gold-bearing fluids were mobilized by devolatilization reactions due to crustal thickening and radiogenic heat (ca. 2600-2580 Ma; Bleeker et al., 2007). Regional M2 metamorphism in the Slave craton is characterized by a final granitoid bloom, the appearance of S-type granites and a strongly foliated deformation fabric (D2; ca. 2600-2580 Ma; Kusky, 1993; Davis and Bleeker, 1999).

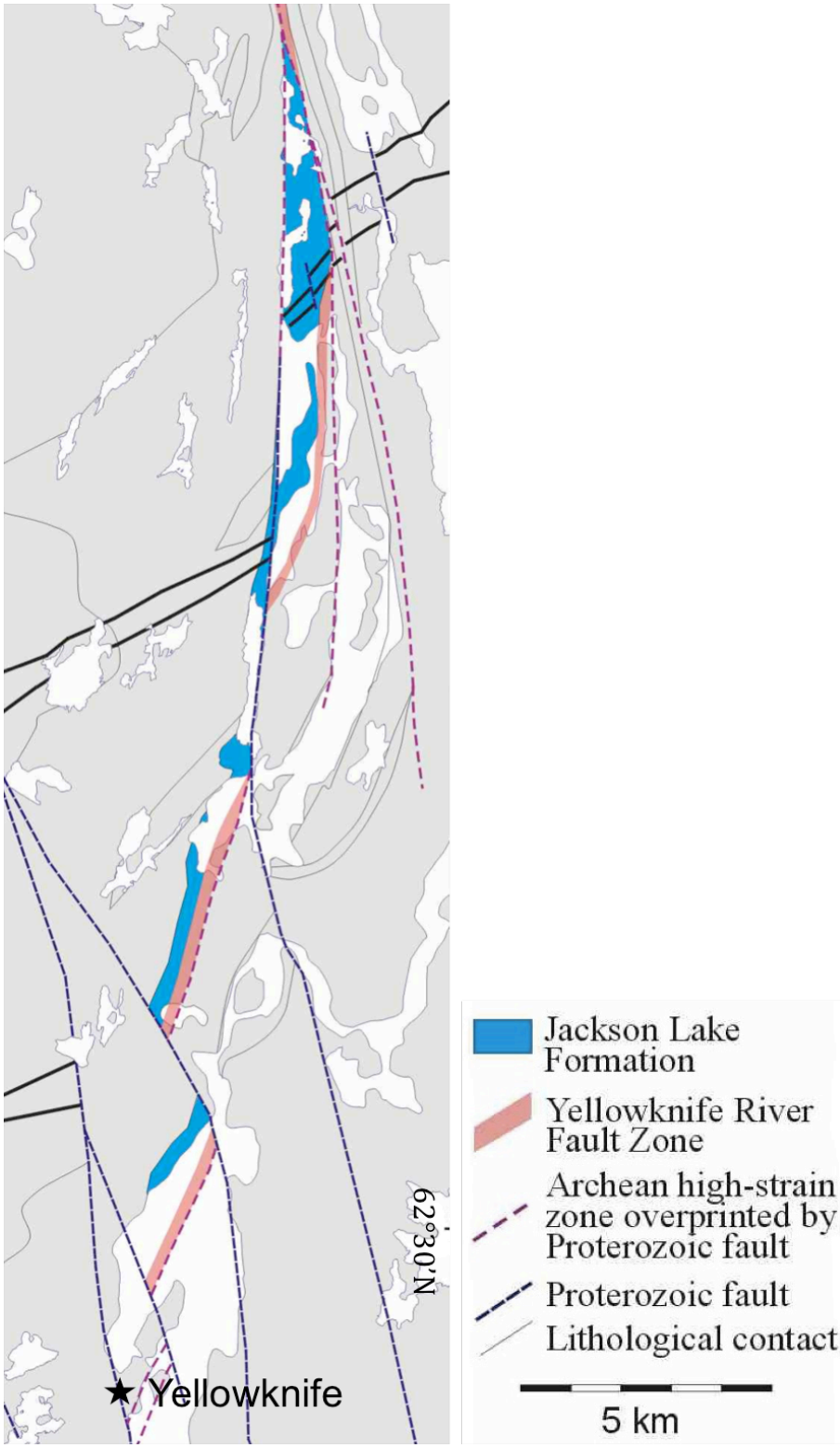

Figure 3. Simplified map of part of the Yellowknife greenstone belt showing the location of the Yellowknife River Fault Zone, modified after Martel and Lin (2006).

Gold mineralization occurring in the 'classic' shear zone-hosted Con and Giant Mine deposits is attributed to regional deformation (D2) concomitant with regional metamorphism (M2). Using structural data, the timing of D2 deformation and M2 metamorphism is estimated at ca. 2590 Ma (Davis and Bleeker, 1999; Siddorn et al., 2006).

Potential Settings for Gold Deposition

Commonly, gold mineralization in the Yellowknife greenstone belt is associated with arsenopyrite and pyrite, and is thought to have formed through a number of mineralizing events over a protracted period of time (Armstrong, 1997; Siddorn et al., 2006). More recently, ages for gold deposition at the Con mine (2591 ± 37 Ma) have been calculated based on the intimate association of pyrite and gold in the YGB using Re-Os geochronology (Ootes et al., 2011). These ages closely reflect proposed ages of high-temperature metamorphism (ca. 2600-2580 Ma) in the YGB suggesting metamorphism and gold mineralization are broadly synchronous (Ootes et al., 2011).

At the Giant mine, although ores were deposited in high-Ti (i.e. ilmenite-rich) metabasalts, it has been suggested that gold-bearing fluids originated, at least in part, in adjacent metasedimentary rocks east of the mine. The Yellowknife River Fault Zone (Fig. 3), a shallow dipping zone which defines the contact for the Kam and Banting Groups, may have acted as a conduit for gold-bearing fluids in the southern portion of the YGB (van Hees et al., 1999). This idea is supported by the large volume of metasedimentary rock in the YGB relative to the limited volume of metavolcanic rocks that host substantial

economic quantities of gold ore (van Hees et al., 1999; Shelton et al., 2004). This implies that metavolcanic host rocks were important geochemically, for precipitation of gold from fluids originating within faulted metasedimentary rocks.

Within the north end of the YGB, metavolcanic rocks are in contact with metasedimentary rocks, frequently associated with faults, suggesting that communication of fluids between these two reservoirs (metavolcanic and metasedimentary) is feasible. Interplay of fluids from these reservoirs has the potential to lead to the development of large gold deposits. I hope to test this idea through geochemical studies of mineralized areas in the north end of the YGB. Conclusions from these studies may be extended to other areas in the YGB (i.e. Ormsby Lake), where metavolcanic rocks are surrounded by metasedimentary rocks and where faults may have acted as conduits for fluids.

CHAPTER II: FIELD OBSERVATIONS AND ORE PETROLOGY

Based on field observations, five important mineralized localities within the basal Chan Formation of the Kam Group and one locality within the overlying Banting Group were selected for detailed study (Fig. 4). Within the Chan Formation, Greyling Lake, Chan Lake, Homer Lake, Oro Lake, and Arseno Lake showings were chosen because they differ significantly in the style and relative age of the mineralization present (Table 1). Among the Banting Group prospects that we sampled, the Ann claims contains the most abundant mineralization, including visible gold, and was chosen as the focus for studies within this younger unit (Table 1). Descriptions of Banting Group mineralization are cited from Hill's (2010) University of Missouri B.S. Thesis, as are additional descriptions of polished thin sections.

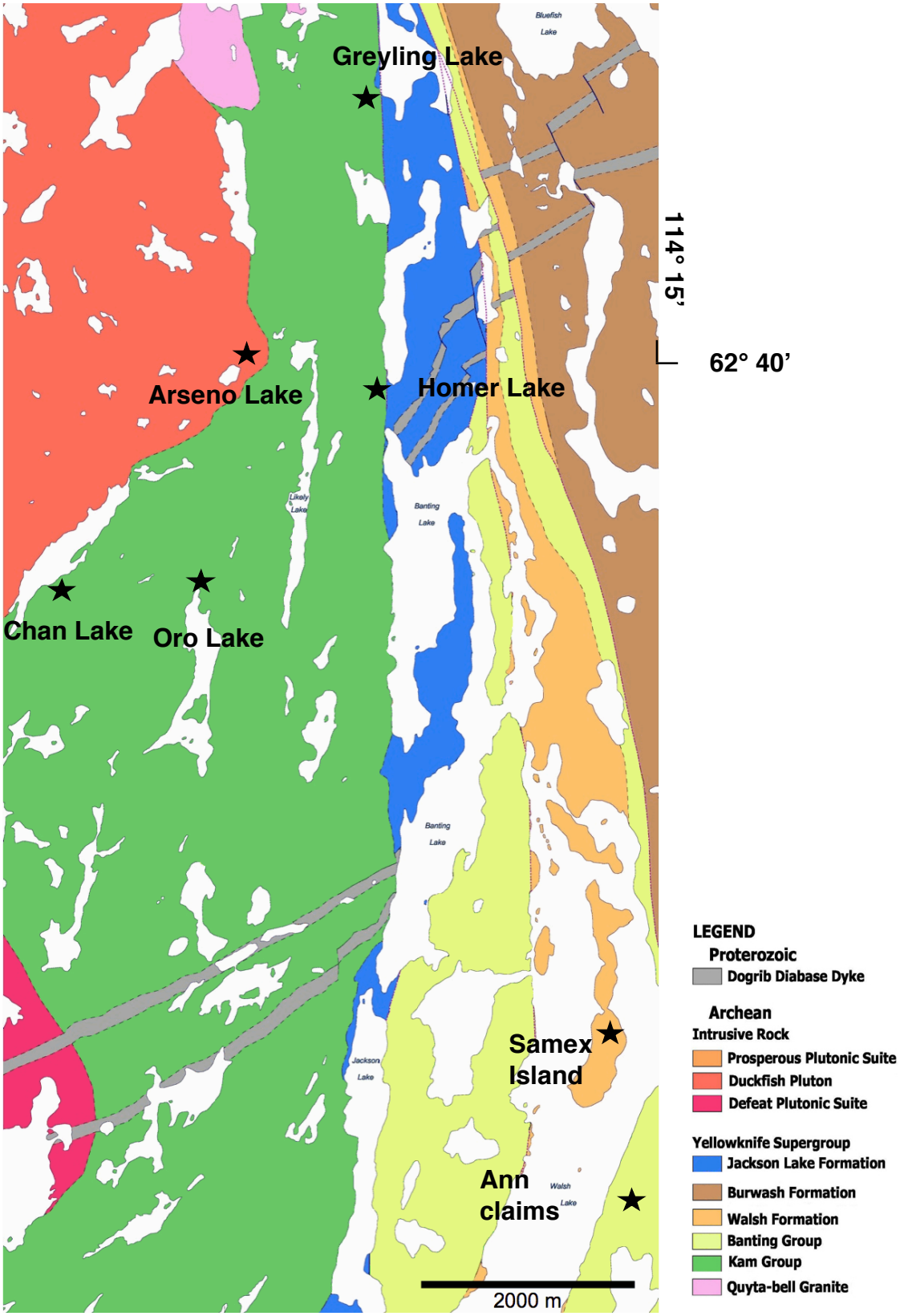
Greyling Lake
Arseno Lake
Homer Lake
Chan Lake
Oro Lake
Samex Island
Ann claims
Bluefish Lake
Likely Lake
Banting Lake
Banting Lake
Jackson Lake
Walsh Lake
114° 15'
62° 40'
2000 m
LEGEND
Proterozoic
Dogrib Diabase Dyke
Archean
Intrusive Rock
Prosperous Plutonic Suite
Duckfish Pluton
Defeat Plutonic Suite
Yellowknife Supergroup
Jackson Lake Formation
Burwash Formation
Walsh Formation
Banting Group
Kam Group
Quyta-bell Granite

Figure 4. Geologic map showing mineralized sample localities, modified after Martel and Lin (2006).

KAM GROUP

Greyling Lake

The Greyling Lake prospect occurs within the Chan Formation and contains a thick lens of massive sulfide extending parallel to the metavolcanic stratigraphy, which appears to be a volcanogenic massive sulfide (VMS) style of mineralization. It is crosscut by later quartz veins. Ore petrology of Greyling Lake massive sulfide samples reveals early arsenopyrite and pyrite replaced by chalcopyrite, galena, and minor pyrrhotite. A skarn-type alteration zone occurs stratigraphically upward from this sulfide lens. This skarn zone may represent a metamorphic overprint of an original carbonate alteration associated with original emplacement of the sulfides (Figs. 5 and 6). The VMS-style of this mineralization suggests that sulfides pre-date regional metamorphism (M2) and are approximately the same age as the adjacent mafic rocks (>2738 Ma based on a cross-cutting dike at Homer Lake, J. Ketchum, unpublished data; in Bleeker and Hall, 2007).

Chan Lake

At Chan Lake, a pink, sucrosic quartz vein, up to 1.5 m wide, associated with potassic alteration, crosscuts a granitic intrusion (2608 Ma; Davis et al., 2004). Ore petrology of Chan Lake samples reveals early arsenopyrite and pyrite replaced by chalcopyrite, pyrrhotite, and minor sphalerite.

Figure 5. Near-vertical lens of VMS mineralization (outlined in red) with skarn alteration at Greyling Lake. Hammer is approximately 30 cm in length.

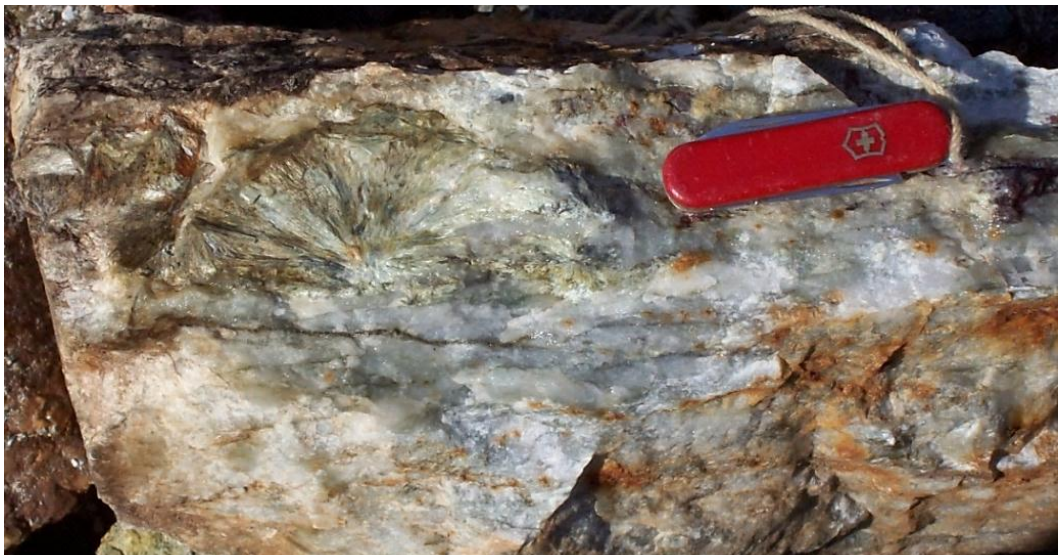

Figure 6. Skarn mineralization with large actinolite spray from Greyling Lake. Knife is approximately 5 cm in length.

Homer Lake

At Homer Lake, generally northeast-trending shear zones crosscut metavolcanic rocks of the Chan Formation. These mineralized shear zones are younger (perhaps significantly) than those seen at Greyling Lake. Massive sulfide zones and quartz veins occur at intersections of shear zones and are characterized by an early arsenopyrite-bearing stage and a later base-metal sulfide overprint. The Homer Lake area also contains an unusual style of late mineralization in which quartz grains appear to have been milled in a matrix of base-metal sulfides, referred to as durchbewegung texture (Marshall and Gilligan, 1989).

Reflected light microscopy of Homer Lake samples reveals early, euhedral to subhedral arsenopyrite and pyrite. Minor pyrrhotite is present as inclusions in both pyrite and arsenopyrite. Sphalerite, galena, and marcasite and less frequently chalcopyrite comprise a late base-metal event and were observed filling fractures and interstices in early arsenopyrite and pyrite grains (Fig. 7).

Reflected light and SEM analysis did not reveal the presence of native gold in our Homer Lake samples. However, review of assay data from NTGO archives indicated ppm-level gold at Homer Lake. We conclude that the gold may be contained within the sulfide minerals themselves or that native gold-bearing horizons were not sampled.

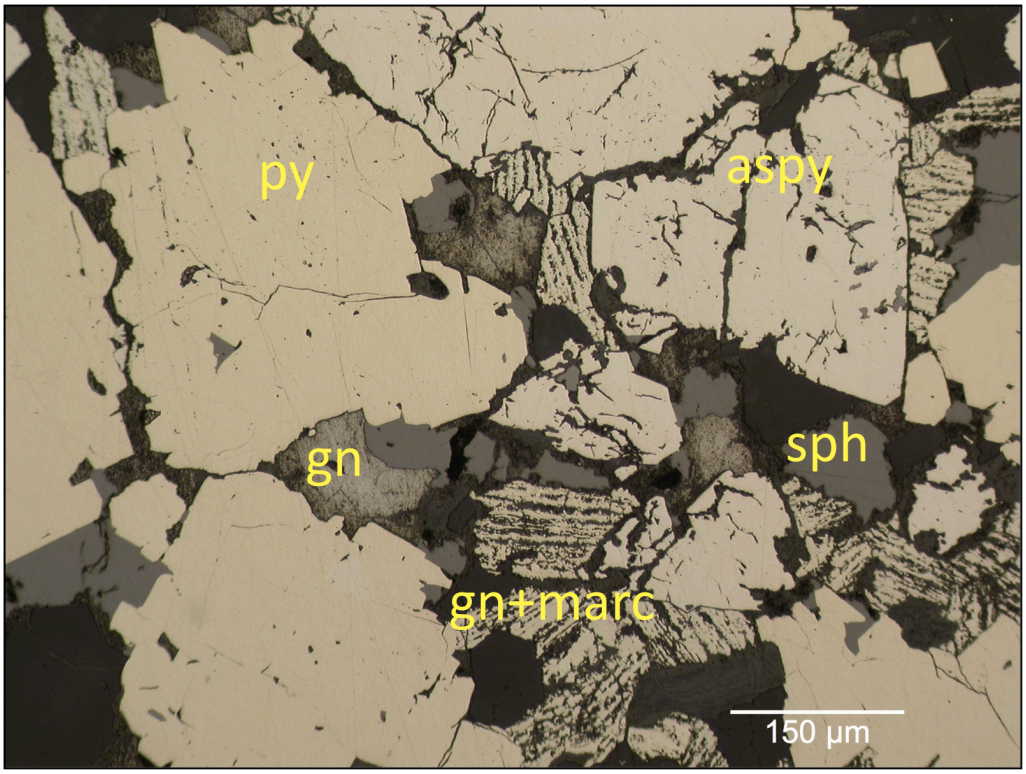

Figure 7. Reflected light photomicrograph of massive sulfide from Homer Lake. aspy=arsenopyrite, gn=galena, marc=marcasite, py=pyrite, sph=sphalerite.

Oro Lake

At Oro Lake, northeast-trending mineralized shears, similar to those seen at Homer Lake, have been overprinted by the Duckfish granite aureole (2608 Ma, U-Pb on zircon; van Breemen et al., 1992). Amphiboles can be seen growing across the shear zones and in quartz veins, confirming a pre-intrusion age for the sulfide mineralization.

Investigation under reflected light reveals abundant chalcopyrite with minor covellite within fractures. This copper mineralization surrounds, and to some degree replaces, early euhedral arsenopyrite and pyrite crystals. Sphalerite is also present as fracture fillings and as a replacement phase in arsenopyrite (Fig. 8). Native gold was observed in altered wall rock at Oro Lake (Fig. 9).

Arseno Lake

In contrast to those at Oro Lake, shear zones at Arseno Lake are northwest-trending and extend from the metavolcanic rocks of the Chan Formation across the contact into the Duckfish granite (2608 Ma; Bleeker and Hall, 2007). This indicates that the mineralization at Arseno Lake postdates the age of the intrusion. This observation reinforces the idea that multiple ore-forming events, over a protracted period of time, formed the mineralized zones within our study area. Sulfide mineralization at Arseno Lake is dominated by euhedral to subhedral arsenopyrite (with minor pyrite and rare chalcopyrite) hosted in shear zones within altered granite (Fig. 10). The dominance of

arsenopyrite at Arseno Lake distinguishes this prospect from other Chan Formation (Kam Group) localities.

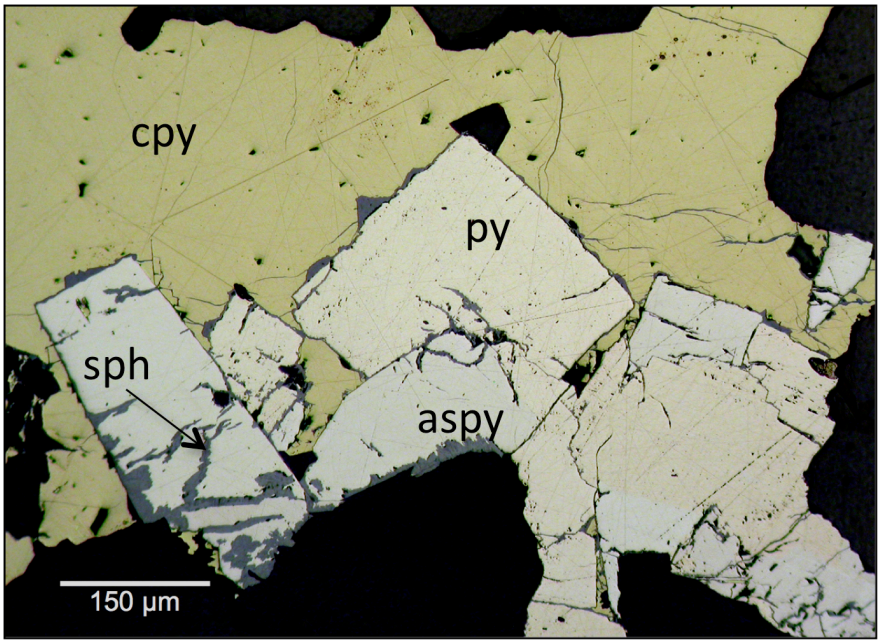

Figure 8. Reflected light photomicrograph of copper-rich mineralization from Oro Lake. aspy=arsenopyrite, cpy=chalcopyrite, py=pyrite, sph=sphalerite.

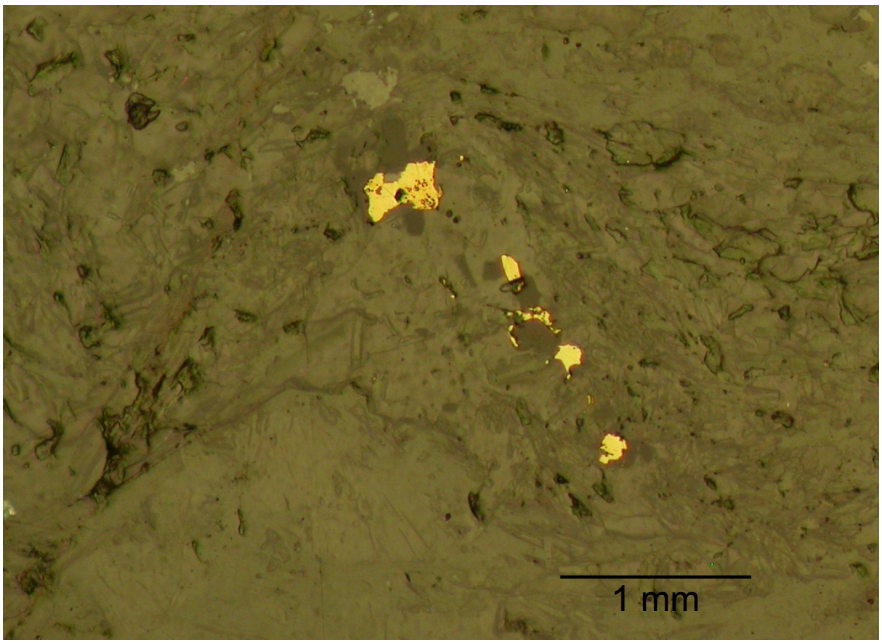

Figure 9. Reflected light photomicrograph of native gold (bright blebs) in altered wall rock at Oro Lake.

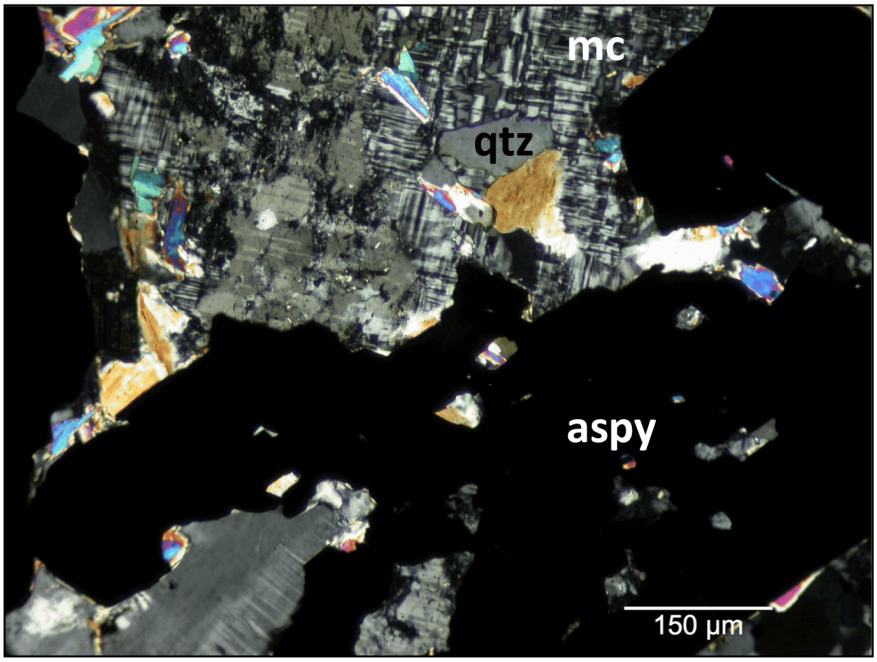

Figure 10. Transmitted light photomicrograph (XPL) of mineralized shear in granite from Arseno Lake. aspy=arsenopyrite, mc=microcline, qtz=quartz.

Showings were also examined near Banting and Walsh Lakes, which are hosted in the stratigraphically younger Banting Group. Samples from these showings provide a basis for comparison of mineralization styles and chemistries with those hosted in the basal Chan Formation of the Kam Group.

BANTING GROUP

Ann claims

In the largest trenched area at the Ann claims, an early arsenopyrite-bearing quartz vein striking 215 to 225°, and dipping 85°NE, is crosscut by a late, well-defined, base-metal sulfide vein that strikes 45° and dips 65°SE. We did not observe this distinct crosscutting relationship in the Kam Group (Chan Formation) showings, where, instead, late sulfides were observed to replace and fill interstices in earlier mineralization or to fill smaller subparallel veins within reopened quartz-arsenopyrite veins.

At the Ann claims (Fig. 4), early arsenopyrite is abundant, with lesser pyrite, and occurs in quartz veins and wall rocks. A later, base-metal overprint is exceptionally pyrrhotite-rich, unlike the Chan-hosted localities that we studied (Fig. 11). Ore petrology of the late base-metal sulfide vein reveals minor euhedral arsenopyrite in a matrix of abundant galena being replaced by sphalerite (Fig. 12).

With reflected light microscopy, small blebs of native gold are seen in samples from this area (Fig. 13). Native gold was found rarely as small (~5 μm) inclusions in early arsenopyrite. More frequently, gold was found as isolated

blebs in veins and in altered wall rock, in which ilmenite has been converted to titanite. SEM studies show that gold occurs along fractures and veinlets in sulfides, which extend outward to larger quartz veins (see Chapter VI). These observations indicate at least two periods of gold deposition in the Banting Group. SEM studies confirm the association of gold with ilmenite/titanite alteration (Fig. 14; see Chapter VI).

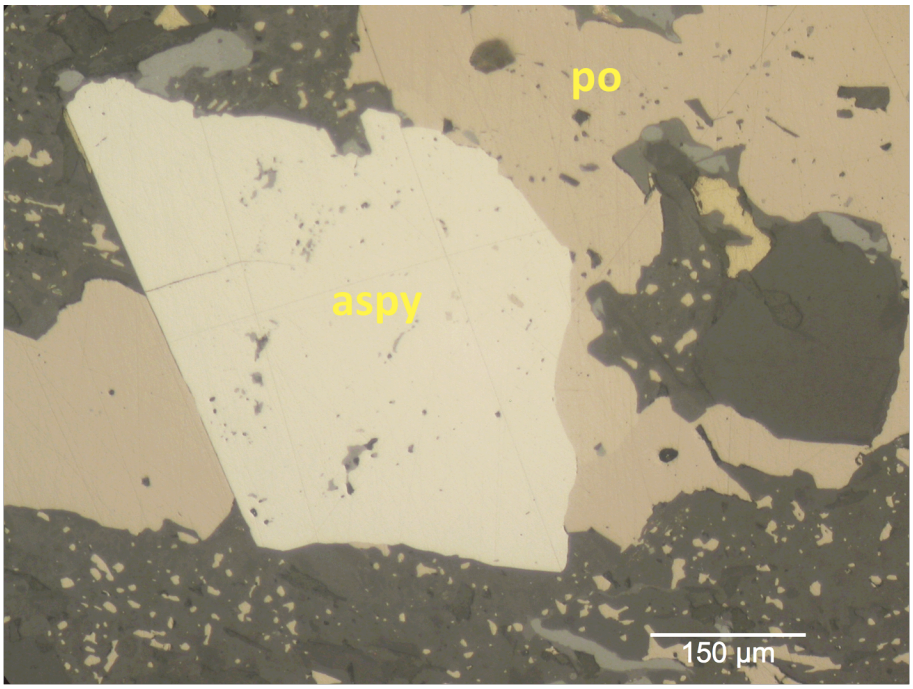

Figure 11. Reflected light photomicrograph of pyrrhotite-rich mineralization in wall rock samples from the Ann claims. aspy=arsenopyrite, po=pyrrhotite.

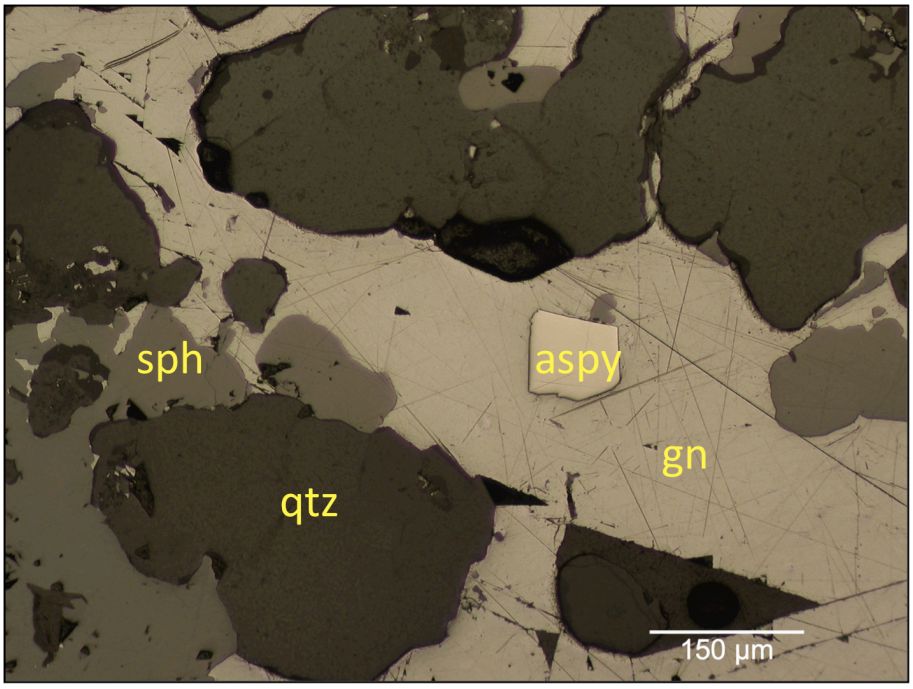

Figure 12. Reflected light photomicrograph of mineralization from base-metal sulfide vein at the Ann claims. gn=galena, qtz=quartz, sph=sphalerite.

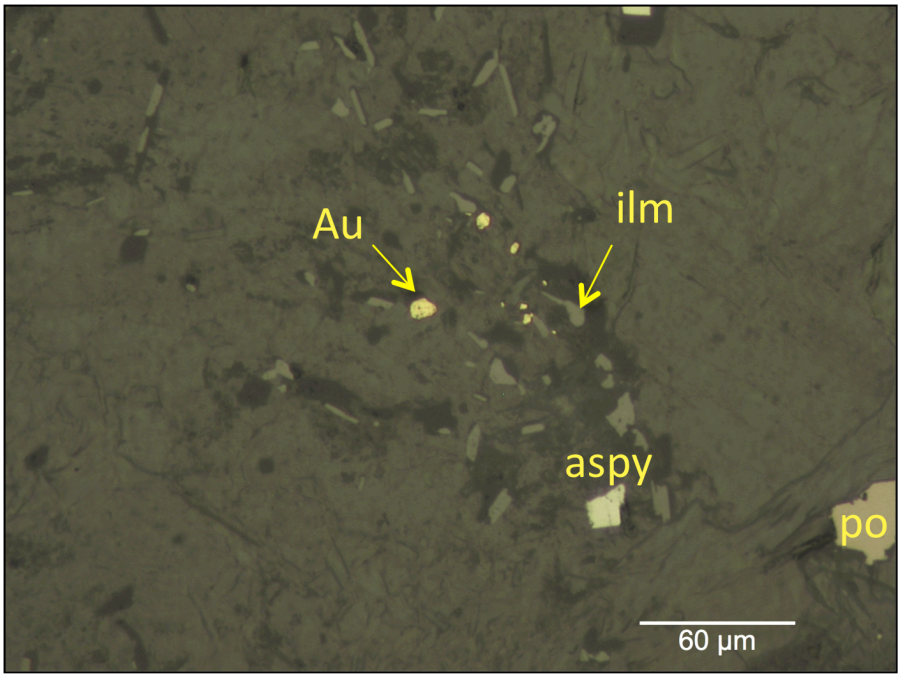

Figure 13. Reflected light photomicrograph of native gold in association with ilmenite, in altered wall rock from the Ann claims. aspy =arsenopyrite, Au=gold, ilm=ilmenite, po=pyrrhotite.

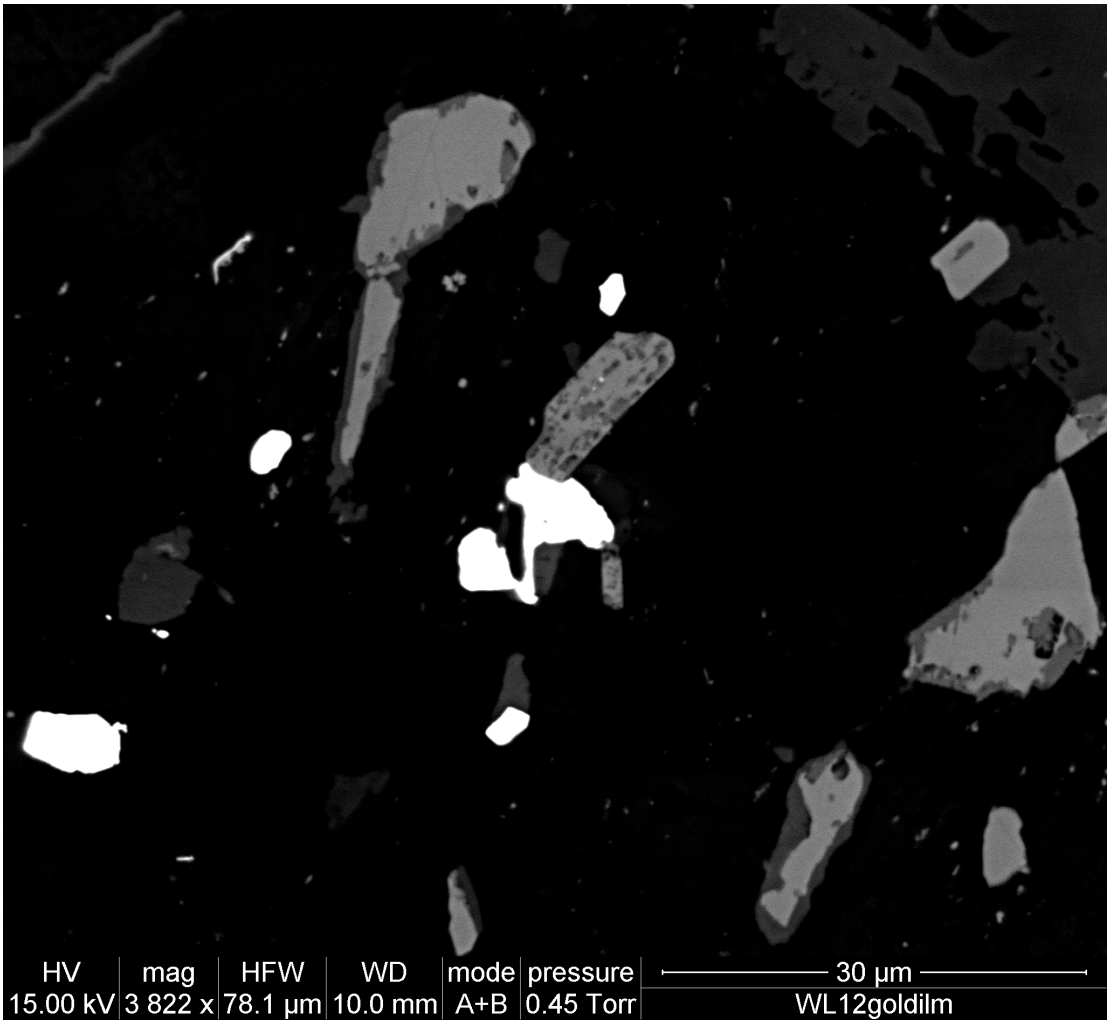

Figure 14. SEM backscatter image of gold (white) in association with ilmenite (light grey) being altered to titanite (dark grey rims) in altered wall rock of the Ann claims.

Samex Island

Ore petrology of samples from Samex Island (Fig. 4) revealed early euhedral arsenopyrite infilled and replaced by abundant pyrrhotite with subordinate chalcopyrite and sphalerite. A later base-metal overprint that is pyrrhotite-rich, similar to the Ann claims, is present. With reflected light microscopy, native gold is observed intergrown with pyrrhotite or occurring as isolated blebs in quartz.

Banting Lake

Sheared mafic metavolcanic rocks at Banting Lake show evidence of a biotite alteration. Blue-gray quartz veins trend parallel to foliation in sheared wall rock. Reflected light microscopy of Banting Lake samples revealed early euhedral arsenopyrite infilled and replaced commonly by abundant pyrrhotite. In altered wall rock, we observed abundant ilmenite needles altering to titanite.

	Locality	Mineralization Present	Relative Age
Banting Group	Ann claims	two stages of Au present; early aspy (containing Au) + lesser py; later Au + po in quartz veins and altered wall rock; latest base-metal overprint is po-rich with gn replaced by sph	
	Samex Island	early aspy infilled and replaced by abundant po with subordinate cpy + sph; Au present in altered wall rock and quartz veins	host rocks are ~ 2679 Ma
	Banting Lake	early aspy infilled and replaced by abundant po	
Kam Group	Greyling Lake	early aspy + py ± Au overprinted and replaced by cpy + gn + minor po	mineralization parallel to metavolcanic stratigraphy (>2738 Ma)
	Homer Lake	early aspy + py ± Au + minor po; late base-metal event of sph + gn + marc ± cpy	mineralized shears crosscut metavolcanic stratigraphy (<2738 Ma)
	Oro Lake	early aspy + py ± Au; late cpy + sph infill and replace early sulfides	mineralization overprinted by 2608 Ma granite aureole
	Chan Lake	early aspy + py ± Au infilled and replaced by cpy + po + minor sph	mineralized veins crosscut 2608 Ma granitic intrusion
	Arseno Lake	aspy + minor py + rare cpy	mineralization crosscuts 2608 Ma granite

Table 1. Summary of mineralization and relative ages of localities in the Kam and Banting Groups; aspy=arsenopyrite, cpy=chalcopyrite, gn=galena, marc=marcasite, po=pyrrhotite, py=pyrite, sph=sphalerite.

CHAPTER III: CATHODOLUMINESCENCE STUDIES

Cathodoluminescence (CL) analysis of quartz and carbonates was conducted to attempt to correlate mineral events regionally. CL patterns may be related to compositional differences associated with mineralizing events or to deformation events. If these patterns can be correlated, it may be possible to outline the aerial extent of particular mineralizing events with the intent of defining the size of fluid systems. We might be able to assess the possibility of fluid communication/interaction, between and among the systems, as interplay of fluids may lead to the development of larger gold deposits in the YGB.

CL of carbonates is dependent on the presence of activators such as Mn^{2+} and quenchers such as Fe^{2+} (Marshall, 1988). The concentration and distribution of manganese and iron, as well as other minor elements acting as quenchers, is responsible for color, zoning, and intensity in CL of carbonates (Marshall, 1988).

CL in quartz may be compositionally driven (e.g., Ti and Al concentration; Muller et al., 2002, Landtwing and Pettke, 2005) or may be the result of deformation (Gotze et al. 2001). In our samples, the intensity of quartz CL is weak and often requires extended photographic exposure times to capture CL behavior. With extended electron bombardment, I observed quartz CL diminishing in intensity and often disappearing completely over time.

Forty-six quartz-carbonate vein samples from the Kam and Banting Groups have been analyzed at the University of Missouri using a CL8200 Mk5-2 Optical Cathodoluminescence System.

CATHODOLUMINESCENCE RESULTS

Quartz: Most quartz in our samples is non-CL, however, some quartz displays weak blue CL that is associated typically with post-mineralization events, such as mechanical deformation and recrystallization.

Dolomite: Dolomite-ankerite in quartz veins of the Kam Group (Chan Formation) exhibits similar CL zoning in mineral showings up to 5 km apart. Within samples from Chan Lake and Greyling Lake, we found a dolomite-ankerite CL stratigraphy consisting of five euhedral zones (Fig. 15a and b). The inner zone is a thick, dark brownish-red zone, and is surrounded by a thin, bright orange-red zone. This thin zone is followed by a thicker, light red-brown zone, which is then surrounded by a thin, bright orange-red zone, and concludes with a thicker red zone containing multiple bands.

We also documented a unique orbicular CL stratigraphy in dolomite-ankerite from base-metal sulfide veins with durchbewegen textures from Homer Lake (Fig. 15c). The CL pattern alternates between dark and bright red zones, with cores of individual crystals exhibiting either dark or bright CL, depending on the relative timing of their initial growth. After initial nucleation and growth, these orbicular carbonates were evidently large enough that they impinged upon one another and subsequent carbonate growth displays a more continuous CL zoning. At some later time, the carbonates were fractured and their fragments rotated.

In contrast, a reconnaissance study of CL in Banting Group samples found dominantly nonluminescent dolomite-ankerite. Rare, CL-zoned dolomite was

found in some samples from the south end of Banting Lake. These samples display three distinct CL zones. The inner red-orange zone is thick, euhedral, and banded, and is overgrown by a thinner, euhedral, bright red-orange zone. These zones are overgrown by dull dark, red-brown CL carbonate (Fig. 15e).

Calcite: Within the Kam Group at Arseno Lake, we observed dull orange CL calcite filling porosity. This CL stage is overgrown and crosscut by brighter orange CL calcite (Fig. 15d). Bright blue CL potassium feldspar is also crosscut by the bright orange CL calcite. At Homer Lake and Oro Lake, we observed the same dull orange CL calcite, whose fractures are filled by bright orange CL calcites.

This same orange, two-zone CL pattern was observed in calcite in the Banting Group at Walsh Lake (Fig. 15f). The later, bright orange CL calcite was also observed at Banting Lake, where it crosscuts earlier CL-zoned dolomite.

SUMMARY OF CL

Dolomite-ankerite in quartz veins of the Chan Formation (Kam Group) exhibits similar cathodoluminescence zoning (CL) in mineral showings up to 5 km apart. Similar CL zoning is not observed in carbonates in the Banting Group. However, paragenetically later calcite exhibits similar CL patterns in both stratigraphic groups, likely indicating that both groups were affected by a common hydrothermal system during the time of late calcite deposition.

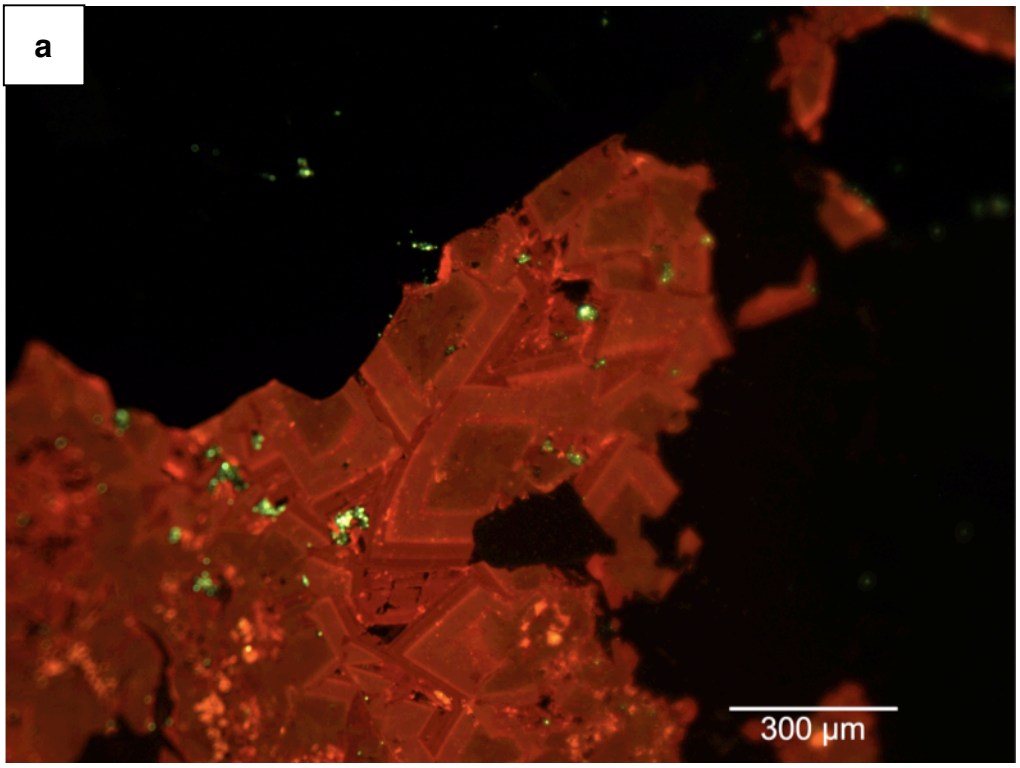
a
300 µm

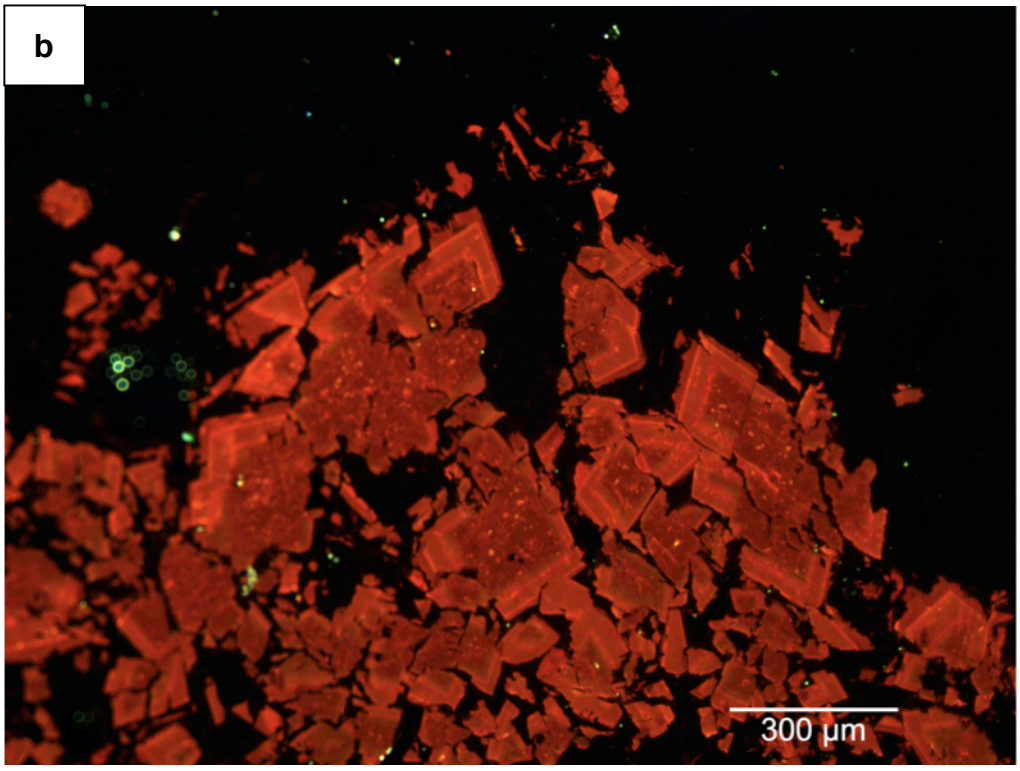
b
300 µm

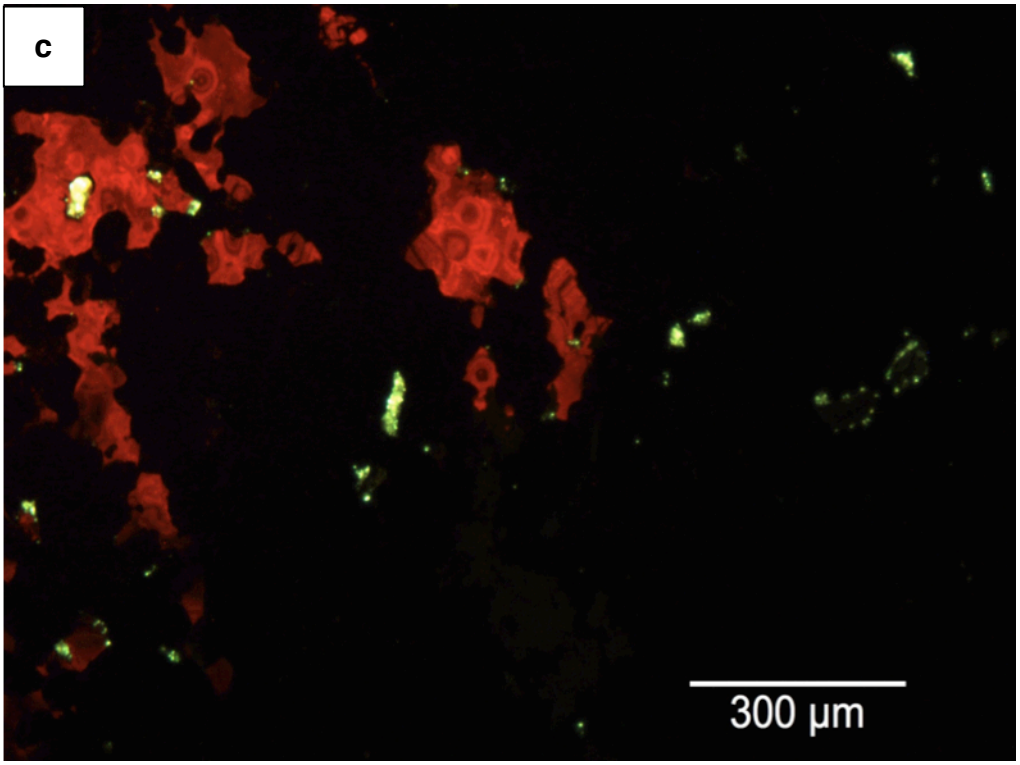
c
300 µm

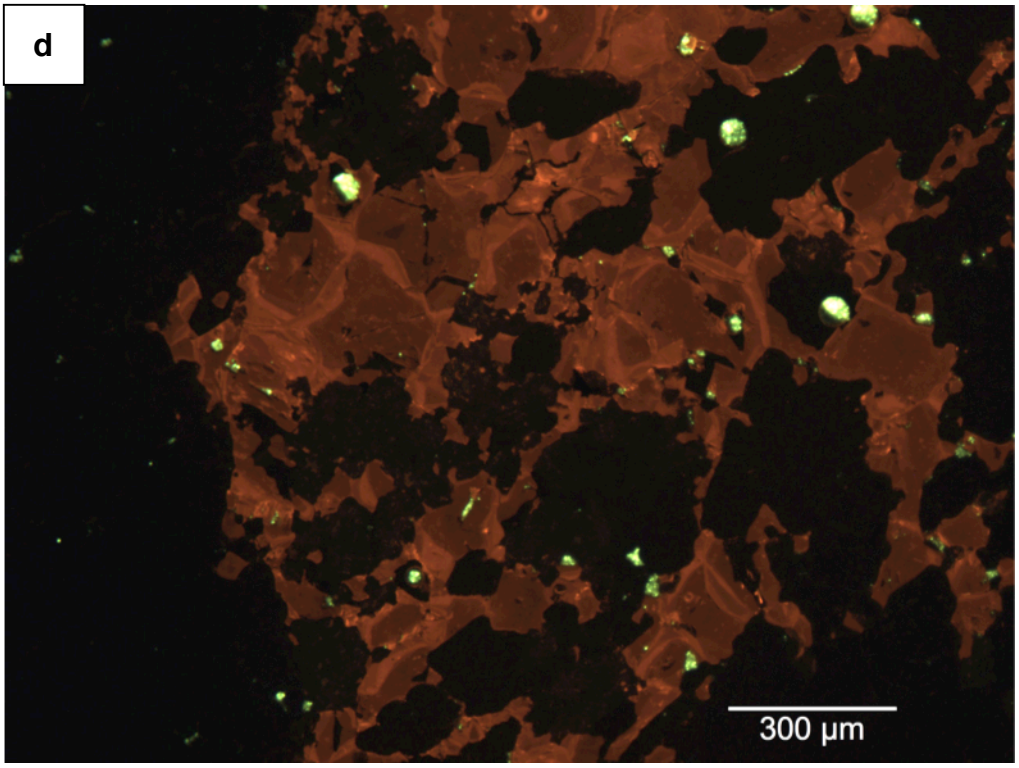
d
300 µm

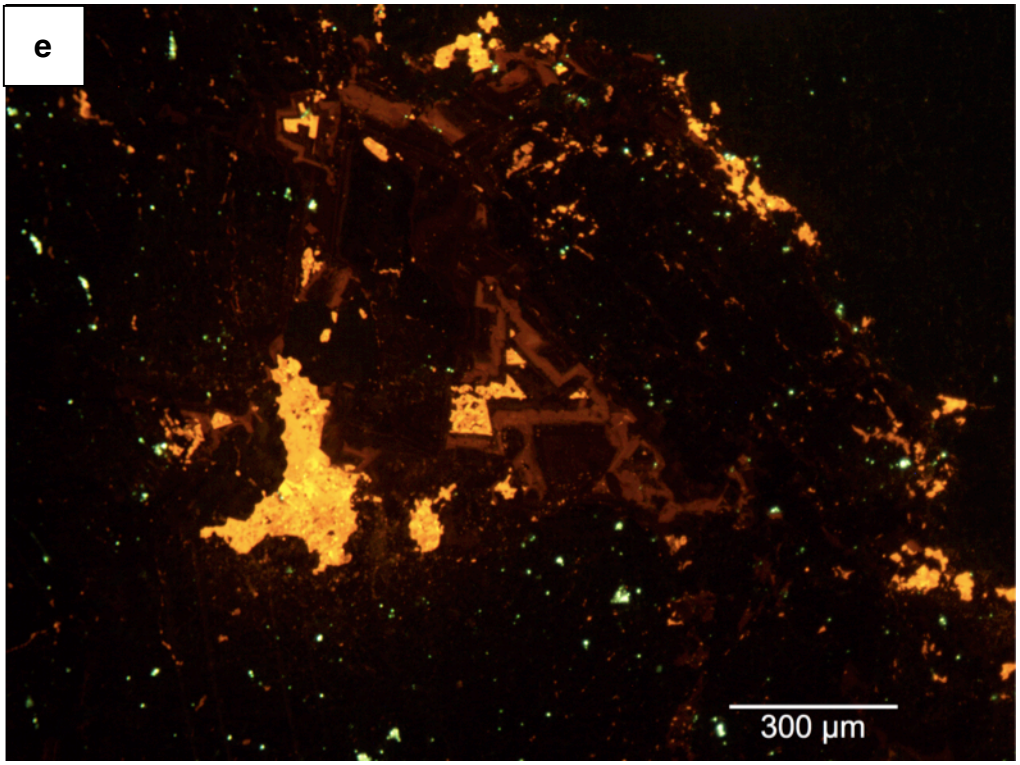
e
300 µm

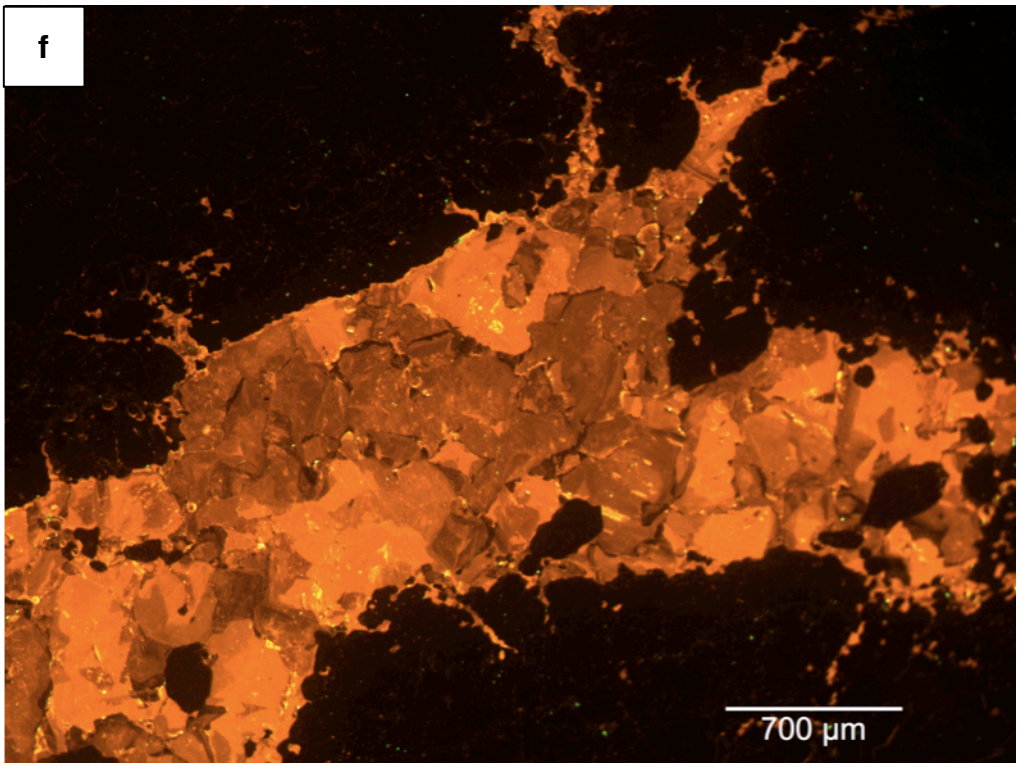
f
700 µm

Figure 15. Cathodoluminescence (CL) photomicrographs of dolomite-ankerite from (a) Greyling Lake and (b) Chan Lake depicting at least five euhedral zones. (c) Homer Lake orbicular CL zoning with alternating dark or light cores. (d) Dull orange CL calcite whose fractures are filled by bright orange CL calcite at Oro Lake. (e) Euhedral CL zoning in dolomite from Banting Lake (Banting Group) that differs from CL zoning found in Kam Group showings (Greyling and Chan Lakes). (f) Two-zoned CL pattern in calcite from Walsh Lake (Banting Group).

CHAPTER IV: FLUID INCLUSION STUDIES

Twenty-six samples of quartz veins from surface exposures in the Kam Group were prepared as standard 120 μm-thick doubly polished sections to determine P-T-X conditions associated with precipitation of quartz and sulfides, relationships among sample localities, and mechanism(s) of ore deposition.

Microthermometric data were obtained using a Linkam THMSG 600 conduction heating/freezing stage. Temperatures of total homogenization (T_h) have errors of <±2°C, and temperatures of melting (T_m of ice, clathrate, and CO_2), solution (T_s of halite), and homogenization of CO_2-rich phases have errors of <±0.2°C. Volume percentages of each phase were estimated visually at room temperature (~20°C).

OCCURRENCE AND COMPOSITIONAL TYPES OF FLUID INCLUSIONS

Fluid inclusions were studied in all styles of quartz veins hosted in metavolcanic rocks of the Chan Formation of the Kam Group and in recrystallized quartz grains from the Duckfish granite. Due to the deformation of the rocks and multiple episodes of fracturing and healing, most fluid inclusions observed are pseudosecondary and secondary. Primary fluid inclusions (H_2O-CO_2 inclusions) were observed only in larger unrecrystallized grains within sheared quartz veins (Fig. 16).

Four compositional types of fluid inclusions have been identified, based on their phase relationships at 20°C and behavior upon cooling. They are, in order

of increasing abundance: carbonic (CO_2±CH_4) inclusions; H_2O-CO_2 inclusions; halite-bearing fluids; and aqueous brines.

Carbonic (CO_2±CH_4) Inclusions

These dark inclusions (Fig. 17a) are dominantly CO_2-rich liquid and are present as isolated inclusions, indicating an initial primary origin. At 20°C, the inclusions consist of one or two phases. Upon cooling, the one-phase inclusions generate a second phase, vapor CO_2. Inclusion shapes vary from regular to negative crystal shapes, and were observed in samples from Arseno Lake and Greyling Lake of the Kam Group.

H_2O-CO_2 Inclusions

These are present as isolated inclusions in quartz, indicating a primary origin (Figs. 16 & 17b). At 20°C, the inclusions consist of two (liquid H_2O + liquid CO_2) or three phases (liquid H_2O + liquid CO_2 + vapor CO_2). Upon cooling, the two-phase inclusions generated a third phase, vapor CO_2. The volume percentage of liquid + vapor CO_2 in these inclusions was typically ~50%, but varied between 20 and 90%. H_2O-CO_2 inclusions were found in samples from Arseno Lake, Homer Lake, Greyling Lake, and Oro Lake and were observed in a reconnaissance study of samples from Samex Island within the Banting Group.

Halite-bearing Aqueous Inclusions

Halite-bearing inclusions are the second most abundant type of fluid inclusion and occur as psuedosecondary or secondary inclusions (Fig. 17c). These three-phase inclusions (liquid H_2O + halite + vapor) were observed in most samples from mineralized areas in the Kam and Banting Groups. Halite-bearing inclusions were also observed in barren quartz veins unrelated to mineralization.

Aqueous Brine Inclusions

These inclusions were found in all samples examined from the Kam Group and were observed in a reconnaissance examination of quartz veins from the Banting Group samples (Fig. 17c). These inclusions are the most abundant type and occur in trails or healed fracture planes that crosscut grain boundaries, indicating a dominantly secondary origin. No primary fluid inclusions of this type were observed. Aqueous brine inclusions range from <5 to ~20μm in size, averaging approximately 5μm. Vapor occupies ~5 to 40 vol.% of each inclusion, though more typically, 5-10 vol.%.

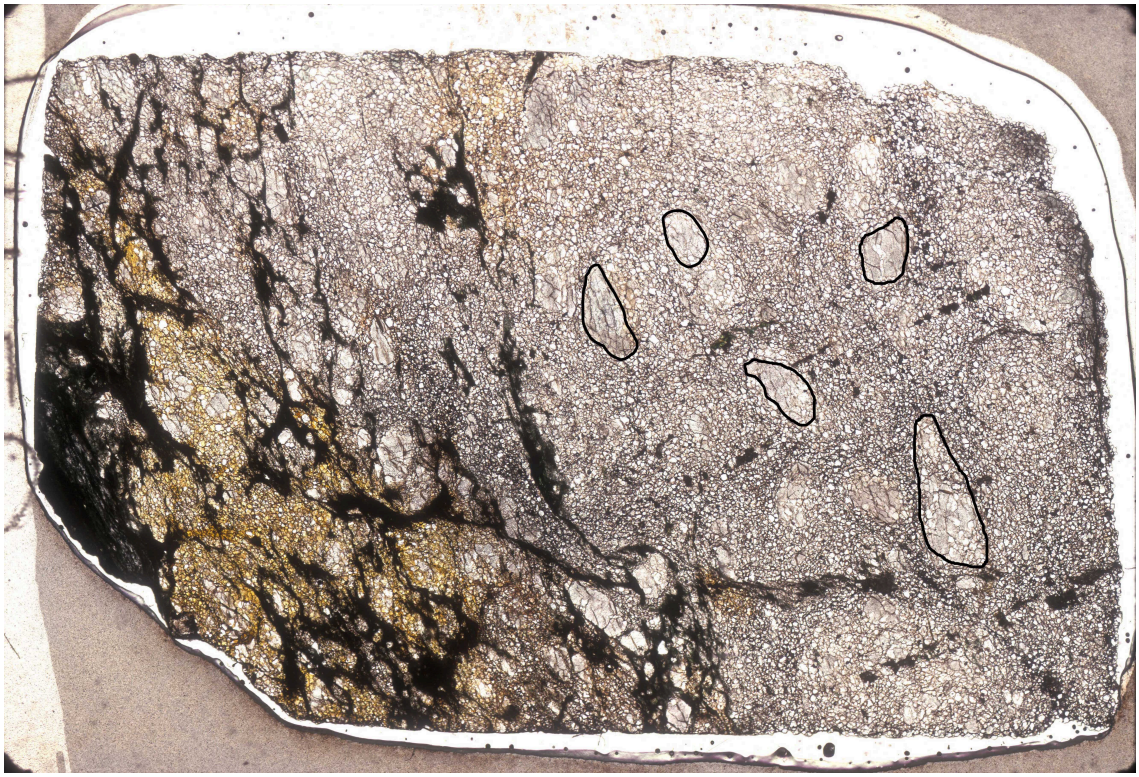

Figure 16. Primary H_2O-CO_2 inclusions are found in larger, relatively undeformed quartz fragments (outlined in black) within sheared and recrystallized quartz veins. Aqueous and halite-bearing fluid inclusions are common within the smaller, more deformed quartz grains. The doubly polished thin section above is from a quartz vein sampled in Trench #11 at Homer Lake, hosted in the Chan Formation of the Kam Group. Width of image is 7.5 cm.

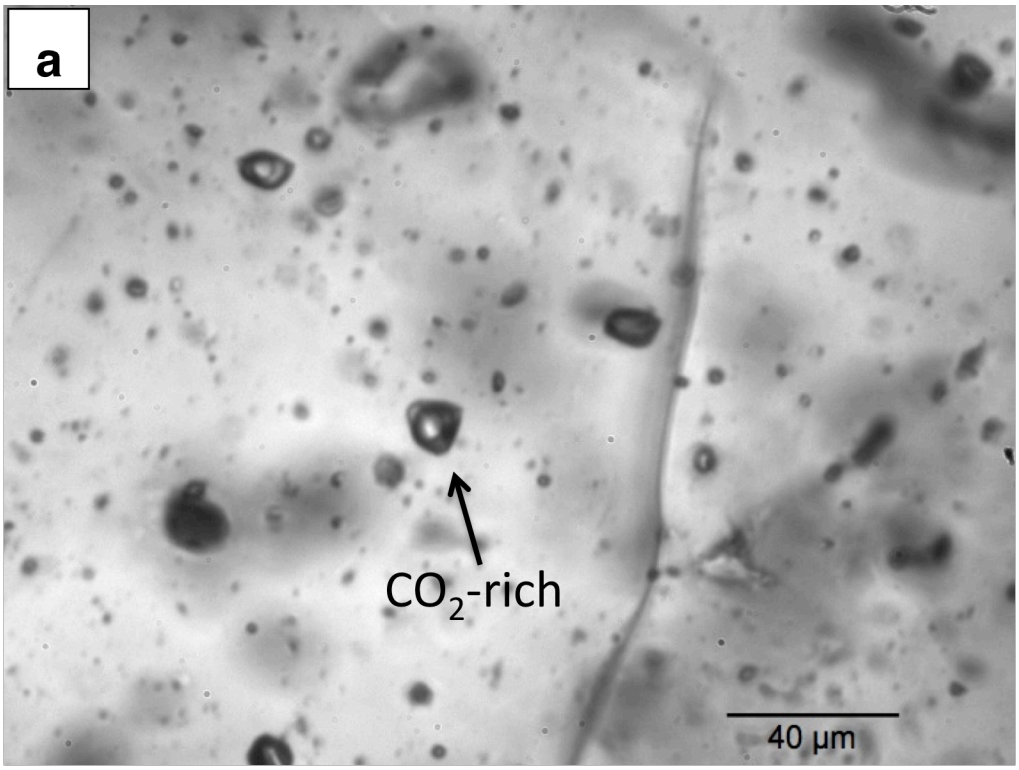
a
CO_2-rich
40 µm

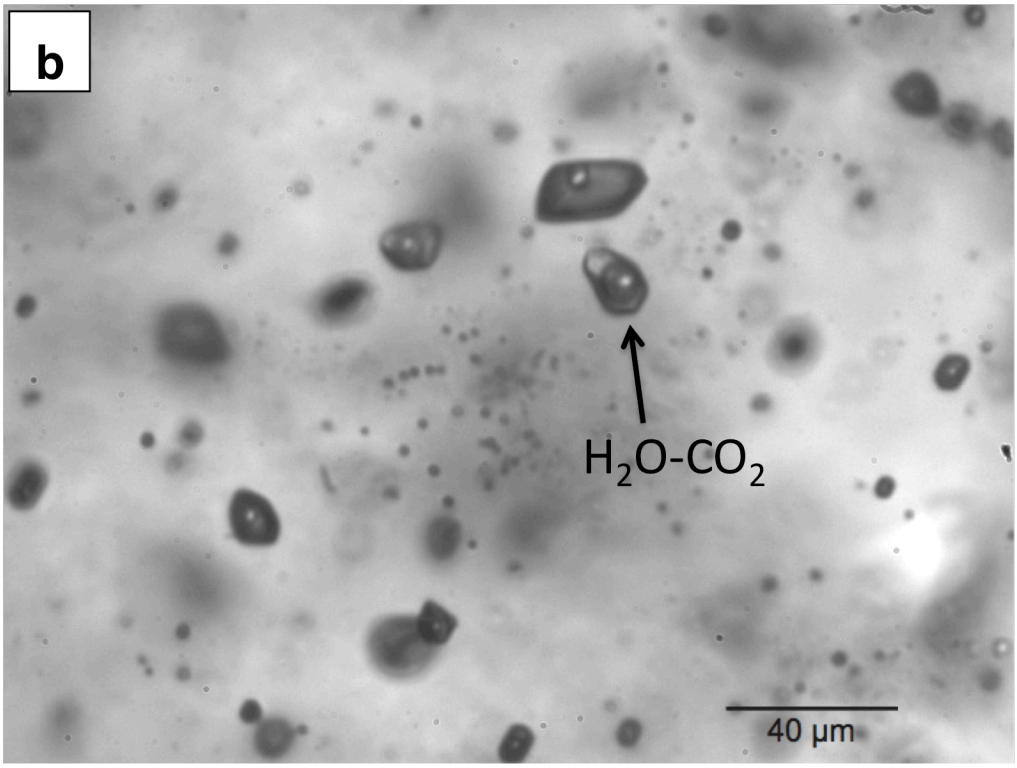
b
H_2O-CO_2
40 µm

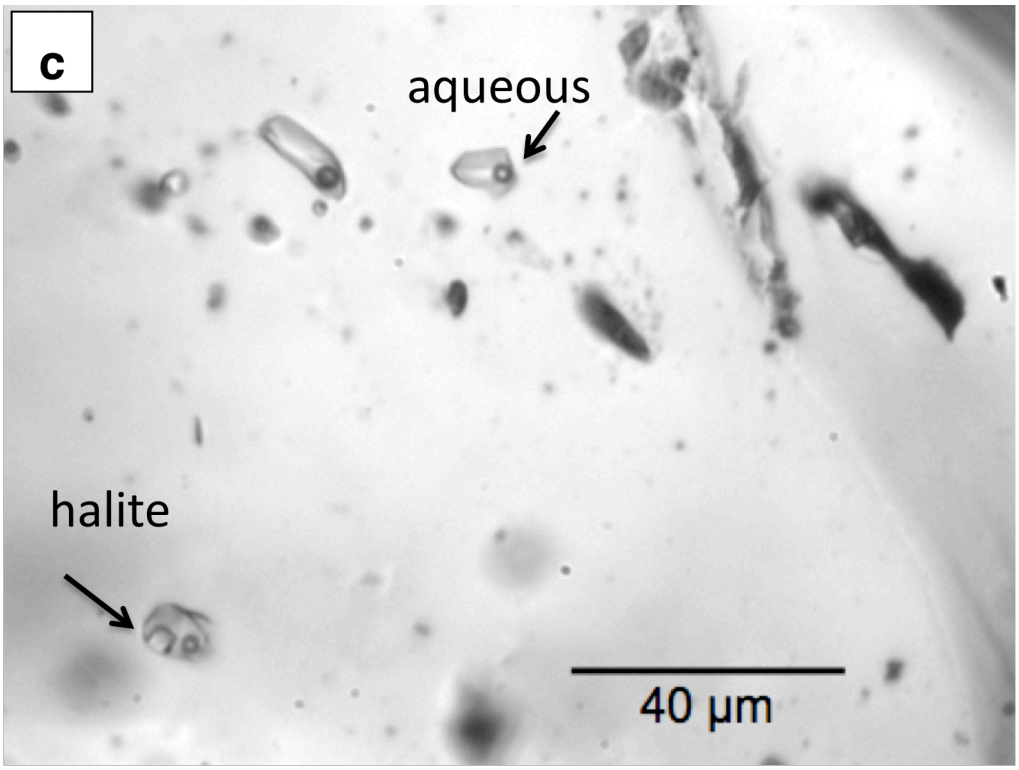

Figure 17. (a). CO_2-rich inclusions occur infrequently and are interpreted to have formed by modification of early H_2O-CO_2 inclusions. **(**b). Primary H_2O-CO_2 inclusions in relatively undeformed quartz grains from Homer Lake. (c). Secondary aqueous brine and halite-bearing inclusions in healed fractures in mechanically deformed quartz.

HEATING AND FREEZING DATA

In total, 41 carbonic and H_2O-CO_2 inclusions and 141 aqueous brine and halite-bearing inclusions were analyzed. Compositions and densities of the trapped fluids were determined from thermometric data using the MacFlinCor software (Brown and Hagemann, 1995) and compiled data of Kerrick and Jacobs (1981), Bodnar and Vityk (1994) and Thiery et al. (1994). Clathrate values were calculated up to only 10°C, because of the limits of the MacFlinCor program.

Carbonic (CO_2±CH_4) Inclusions: Carbonic inclusions have final melting of the solid CO_2 ($T_{m\ CO2}$) from -58.3° to -56.6°C, corresponding to XCH_4 values of 0.06 to 0.00, respectively. Homogenization of CO_2 ($T_{h\ CO2}$) to the liquid phase occurs from 15.4° to 30.9°C. The wide range of $T_{h\ CO2}$ values reflect variable densities of 0.82 to 0.52 g/cc.

H_2O-CO_2 Inclusions: H_2O-CO_2 inclusions have $T_{m\ CO2}$ values of -59.7° to -56.6°C. These values correspond to XCH_4 values of 0.14 to 0.00, respectively, in the carbonic portion of the inclusions (0.02 to 0.00 in the total inclusion fluid). Homogenization of the CO_2 to the liquid phase was dominant, and $T_{h\ CO2}$ values range from 16.1° to 30.9°C. These values yield densities of 0.51 to 0.47 g/cc for the carbonic portion (0.80 to 0.86 g/cc for the total inclusion fluid).

Most H_2O-CO_2 inclusions were too small to observe homogenization. Many H_2O-CO_2 inclusions decrepitated just before anticipated total homogenization. Decrepitation or homogenization to the liquid phase occurred at temperatures ranging from 316° to 449°C. In total, fourteen T_h values were

obtained. Clathrate melting temperatures range widely (from <-10° to >10°C), indicating a range of salinities from 6.7 to ~21.4 wt.% equiv. NaCl.

Halite-bearing Aqueous Inclusions: Halite-bearing inclusions have T_h values that form two distinct groups (Fig. 18). A lower temperature population ranges from 115° to ~180°C, and a higher temperature one ranges from 200° to 270°C. Halite-dissolution temperatures are 115° to 270°C, corresponding to salinities of 28.4 to 36.1 wt.% NaCl (Fig. 19).

Aqueous Brine Inclusions: Aqueous brine inclusions have first ice-melting temperatures (T_e, eutectic temperatures) near -33°C, indicating complex brines that likely contain $CaCl_2$ in addition to NaCl (Zhang and Frantz, 1989). Final ice melting temperatures ($T_{m\ ice}$) are typically near -17°C, corresponding to salinities of ~20 weight % equivalent NaCl. Homogenization to the liquid phase (T_h values) of aqueous brines range from 103° to 392°C (Fig. 18). The T_h values form two populations. Eighty percent of the data define a lower temperature population between 110° to 250°C. The remainder of the data form a minor, higher-temperature group from 270° to 400°C.

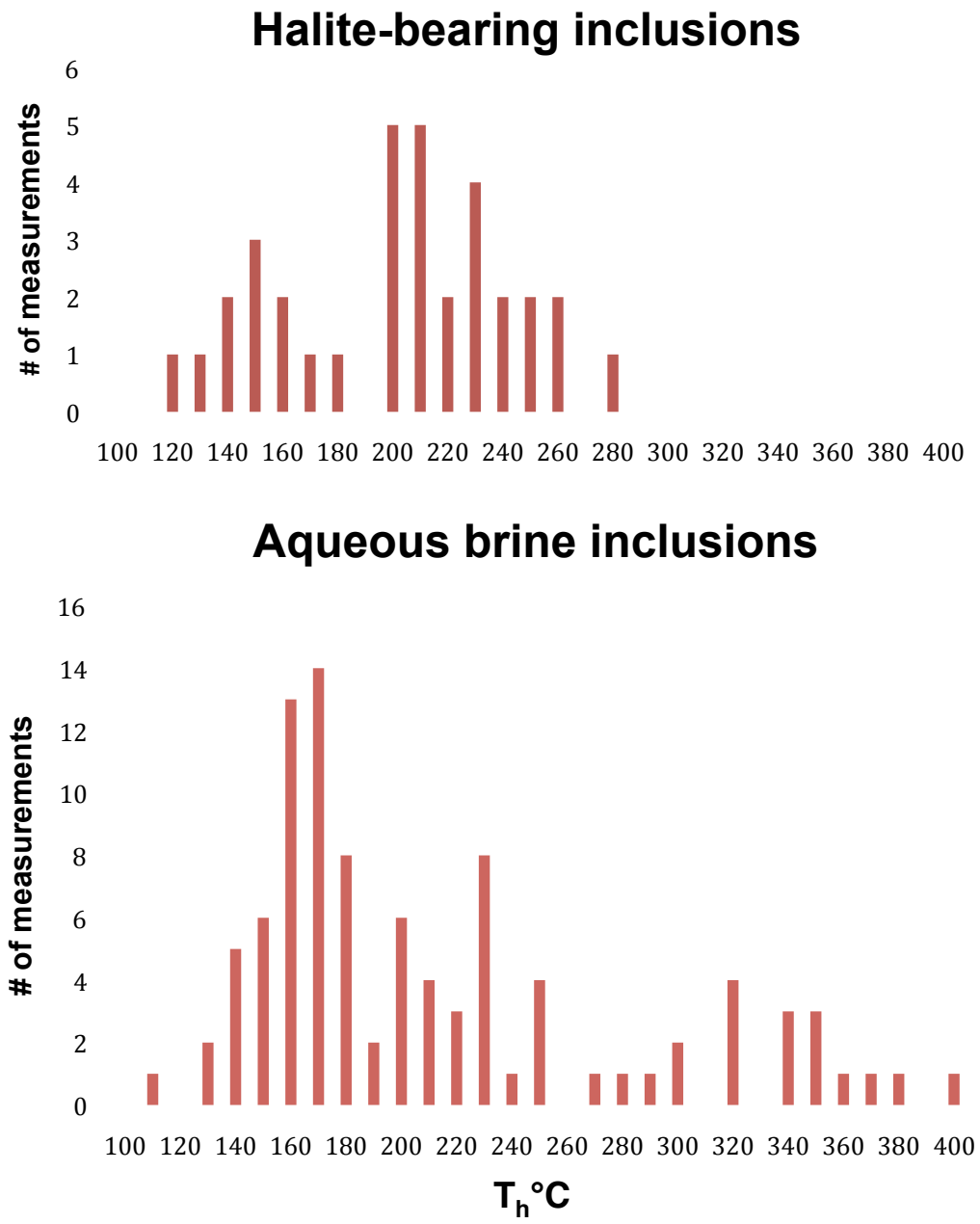

Figure 18. Frequency diagrams of homogenization temperatures (T_h °C) for psuedosecondary and secondary, halite-bearing and aqueous brine inclusions in quartz veins from Kam Group (Chan Formation) showings.

TEMPERATURE-SALINITY VARIATIONS

Figure 19 is a plot of salinity versus T_h for aqueous, halite-bearing, and H_2O-CO_2 inclusions. The vertical axis, wt % equiv. NaCl, is dependent on melting temperature (T_m) of the ice or clathrate, for aqueous and H_2O-CO_2 inclusions, respectively. For halite-bearing inclusions, the salinity is calculated based on T_s of halite.

Primary H_2O-CO_2 inclusions are thought to represent the ore fluid and define a field of higher T_h-higher salinity values. Aqueous brine inclusions with T_h values above 250°C overlap the field of H_2O-CO_2 inclusions. Aqueous brine inclusions that have lower T_h values (<250°C) define a field whose salinity approaches that of halite-bearing inclusions. These higher salinity, aqueous inclusions are from Greyling Lake and Chan Lake. Halite-bearing fluid inclusions (n=44) plot dominantly along the NaCl saturation curve (Fig. 19). However, six of these inclusions plot slightly below this curve because these inclusions homogenized to the liquid before halite disappearance.

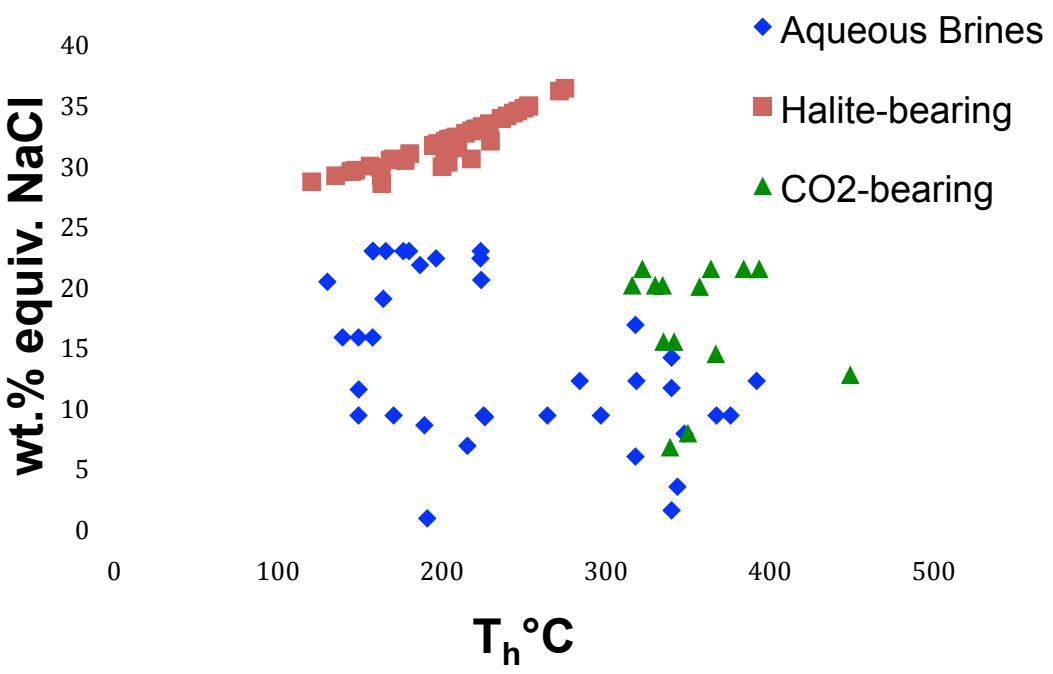

Figure 19. Salinity versus T_h diagram for inclusions in the Chan Formation (Kam Group).

FLUID INCLUSION INTERPRETATION

H_2O-CO_2: Primary H_2O-CO_2 inclusions were found in relatively undeformed quartz grains and their microthermometry yields a narrow range of fluid densities (0.51 to 0.47 g/cc), indicating entrapment at similar conditions. They record temperatures (T_h) of ~315° to 395°C and are thought to represent ore fluids penecontemporaneous with widespread, regional high T-metamorphism (M2) of the host rocks. These H_2O-CO_2-NaCl fluids are similar to primary ore fluids found in other greenstone-hosted gold deposits (Ho et al., 1992; Samson et al., 1997; Shelton et al., 2000, 2004).

Carbonic: The large range of densities determined for carbonic (CO_2±CH_4) inclusions (0.52 to 0.82 g/cc) recorded in the same samples, precludes them from reliably reflecting primary conditions of ore formation. These inclusions are interpreted to have formed by modification of early H_2O-CO_2 inclusions. These carbonic fluid inclusions can form by various processes, including post-entrapment, deformation-recrystallization, such as crystal-plastic deformation and grain-boundary migration recrystallization, which favor trapping of CO_2-bearing inclusions (Bakker and Jansen, 1990; Hollister, 1990; Craw and Norris, 1993; Johnson and Hollister, 1995).

Aqueous Brines: Aqueous-brine (NaCl-$CaCl_2$-H_2O) and halite-bearing inclusions were found as secondary inclusions in healed fractures and were not found to be associated texturally with primary H_2O-CO_2 inclusions or CO_2-rich inclusions. Both of the former inclusion types are ubiquitous in the Kam and Banting Groups, in both mineralized and barren quartz veins, and are considered

post-ore fluids. T_h values for aqueous brine inclusions are dominantly 110° to 250°C, with a minor higher temperature population >270°C, indicating multiple periods of brine entrapment. The higher temperature inclusions could possibly be related to deposition of base-metal sulfides that postdate arsenopyrite-pyrite-gold mineralization. Alternatively, these inclusions could reflect post-ore fluids, similar to those found in the Proterozoic West Bay Fault to the south (Ripple et al., 2009).

The lower-temperature aqueous brines are similar to those found in other parts of the YGB and Slave province: (1) in gold-bearing quartz veins of the Giant mine (Shelton et al., 2004); (2) in quartz veins from shear zones on the Mirage Islands, 25 km south of Yellowknife, where the southernmost exposures of the Yellowknife greenstone belt occur (Relf, 1988); (3) in gold-bearing quartz veins from metasedimentary rocks of the Yellowknife Supergroup (10–12 km northeast, 85 km northeast, and 90 km east of Yellowknife; English, 1981); and (4) in gold-bearing quartz veins from the Colomac mine, located 220 km north of Yellowknife within the Indin Lake supracrustal belt (Shelton et al., 2000). A common origin is supported by the fact that all of these areas have been transected by Proterozoic fault systems.

Halite-bearing: Halite-bearing inclusions occur in the same samples, and frequently in the same healed fractures, as aqueous brine inclusions. Halite-bearing inclusions were also observed in samples from the Banting Group. Halite-bearing inclusions record temperatures (T_h) of ~120° to 280°C, similar to the lower-temperature aqueous brine inclusions. These fluids are interpreted to

be unrelated to the ore fluids and no textural relationships to H_2O-CO_2 inclusions were observed in our samples.

Similar secondary, halite-bearing inclusions were observed in late-stage quartz veins to the south within the Proterozoic West Bay Fault zone (Ripple et al., 2009) and to the west in quartz veins of the Colomac mine associated with the Proterozoic Indin Fault (Costello, 1999). These highly saline fluids may represent a regional brine event associated with reactivation of similar faults that affected both the Kam and Banting Groups.

CHAPTER V: OXYGEN ISOTOPES

Twenty samples of quartz veins from the Kam and Banting Groups were collected for oxygen isotope studies. These samples were representative of all mineralization stages and veins types. For comparison, samples were also taken from barren quartz veins. Samples were separated by hand, crushed, and sieved between 60 and 115 Tyler mesh sizes and analyzed following the procedures of Clayton and Mayeda (1963) at the New Mexico Institute of Mining and Technology.

Oxygen isotope data are presented in standard delta notation relative to Vienna Standard Mean Ocean Water (V-SMOW). The standard error of each analysis is ±0.2‰. Oxygen isotope compositions may provide information on fluid sources and fluid interactions with rocks along flow paths, as well as similarity of fluids among different vein sets.

Ranges of equilibrium $\delta^{18}O_{water}$ values responsible for quartz vein precipitation were calculated using the quartz-water curve of Clayton et al. (1972) and a temperature range of 350° to 400°C, based on fluid inclusion homogenization temperatures. The corresponding $\delta^{18}O$ values show permissible ranges for $\delta^{18}O_{water}$ values.

Quartz veins hosted in mafic metavolcanic rocks of the Kam Group (Chan Formation) at the Chan Lake, Greyling Lake, Homer Lake, and Oro Lake mineralized areas have $\delta^{18}O$ values of 10.0 to 11.8‰ and yield calculated $\delta^{18}O_{water}$ values of 4.2 to 7.3‰ (n=16; Table 1). Quartz in veins from Banting Group rocks (Ann claims, Banting Lake, Kingfisher Island, and Samex Island)

has $\delta^{18}O$ values of 13.2 to 14.8‰, and yield calculated $\delta^{18}O_{water}$ values of 7.4 to 10.3‰, (n=5; Table 1). Recrystallized quartz from the main showing at Arseno Lake, which is hosted in the Duckfish granite, has a $\delta^{18}O$ value of 8.3‰ and yields calculated $\delta^{18}O_{water}$ values of 2.5 to 3.8‰ (n=1; Table 2).

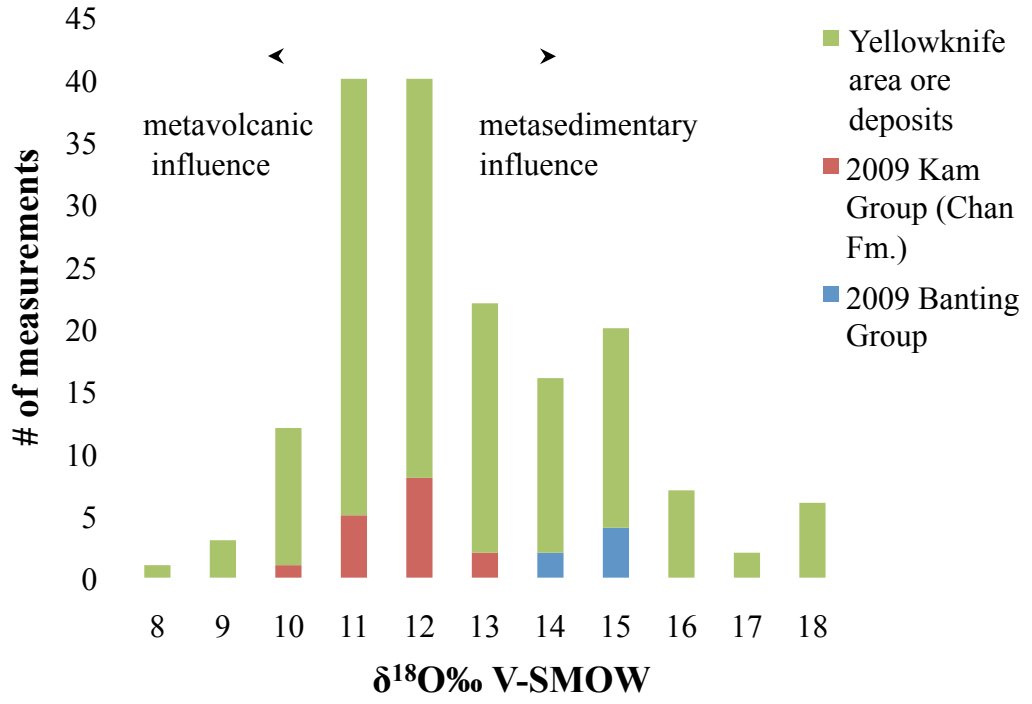

Figure 20. Frequency diagram of $\delta^{18}O$ values of quartz veins in mineralized areas of the Kam Group (Chan Formation) and Banting Group. In addition to our samples, this diagram shows values from other deposits in the Yellowknife District (Kerrich and Fyfe, 1981; van Hees et al., 1999; Shelton et al., 2004).

	SAMPLE	$\delta^{18}O_{quartz}$	$\delta^{18}O_{water}$ 350°C	$\delta^{18}O_{water}$ 400°C
Kam Group (Chan Fm.)	CL-09-1	11.0	5.2	6.5
	GL-09-1B	10.0	4.2	5.5
	GL-09-5	11.2	5.4	6.7
	GL-09-8	10.4	4.6	5.9
	HL-09-10A	11.8	6.0	7.3
	HL-09-10B	11.4	5.6	6.9
	HL-09-10D	11.1	5.3	6.6
	HL-09-15	10.8	5.0	6.3
	HL-09-17	11.4	5.6	6.9
	HL-09-2	11.6	5.8	7.1
	HL-09-2 DUP	11.6	5.8	7.1
	HL-09-9	11.3	5.5	6.8
	OL-09-3	10.6	4.8	6.1
	OL-09-4	10.2	4.4	5.7
Banting Group	BL-09-1	14.4	8.6	9.9
	BL-09-4	14.8	9.0	10.3
	SI-09-2	14.6	8.8	10.1
	WL-09-19	13.2	7.4	8.7
	WL-09-19 DUP	13.4	7.6	8.9
	WL-09-3	14.7	8.9	10.2
Duckfish Intrusion	AL-09-7	8.3	2.5	3.8

Table 2. The $\delta^{18}O_{quartz}$ and calculated $\delta^{18}O_{water}$ values (‰ V-SMOW) for veins from mineralized areas of the Kam Group (Chan Formation) and Banting Group. AL= Arseno Lake; BC= Blue Claims; BL= Banting Lake; CL= Chan Lake; GL= Greyling Lake; HL= Homer Lake; OL= Oro Lake; SI=Samex Island; WL= Walsh Lake.

INTERPRETATION AND SUMMARY OF OXYGEN ISOTOPES

The $\delta^{18}O_{quartz}$ and calculated $\delta^{18}O_{water}$ values are distinct for each group (Kam, Banting, and Duckfish Intrusion). The higher values are consistent with fluids that equilibrated with metasedimentary rocks. Lower values are consistent with fluids that equilibrated with metavolcanic rocks. Similar influences of metavolcanic and metasedimentary fluid sources on $\delta^{18}O$ values of quartz veins have been documented regionally within the YGB (Fig. 20; Kerrich and Fyfe, 1981; van Hees et al., 1999; Shelton et al., 2004).

Based on oxygen isotopes and lithogeochemistry, it has been suggested that the major refractory gold ore mineralization in the Giant mine in Yellowknife was the result of metasedimentary fluid interaction with metavolcanic host rocks (van Hees et al., 1999, 2006; Shelton et al., 2004). Our sample localities from the Kam and Banting Groups exhibit no overlap in $\delta^{18}O_{quartz}$ values, indicating distinct fluid-rock reservoirs with no evidence of fluid communication/interaction between them. We speculate that the faults that define the contact between the Kam and Banting Groups did not permit fluid communication between the groups, perhaps because they were more steeply dipping than those of the Yellowknife Fault Zone of the south. If overprinting metasedimentary and metavolcanic hydrothermal systems are a prerequisite for formation of large gold deposits in the YGB, this may explain why no large economic deposits have been found in our study area. Other areas in the YGB may be better candidates to test the interplay between metasedimentary and metavolcanic rock volumes,

where mafic metavolcanic rocks are surrounded by faulted metasedimentary rocks and where faults may provide conduits for fluids (e.g. Ormsby Lake).

CHAPTER VI. SCANNING ELECTRON MICROSCOPY

Scanning electron microscopy (SEM) was conducted at the University of Missouri, using an FEI Quanta 600 FEG Extended Vacuum Scanning Electron Microscope equipped with an energy dispersive spectrometer (EDS). Samples were uncoated and analyzed at low vacuum, using an accelerating voltage of 15 kV to 30 kV, and a beam current of ~30 μA. Backscatter images and secondary electron images were taken of various mineral phases. EDS was conducted on samples from Kam and Banting Group localities to determine compositional variations within sulfides; to determine host phases for gold in sulfides and/or in altered wall rock; and to help identify smaller unknown mineral phases.

Sphalerite

Sphalerite is present in samples from both the Kam and Banting Groups and represents part of a late-stage base-metal event. Within the Kam Group, sphalerite was often observed infilling fractures and/or replacing grain boundaries within early arsenopyrite and pyrite along grain boundaries (Fig. 21) or as larger crystals floating within a matrix of galena (Fig. 22). Within the Banting Group, sphalerite was often observed infilling fractures in early arsenopyrite and later pyrrhotite and/or intergrown with galena.

Elemental compositions of sphalerite were determined for samples from the Kam and Banting Groups**.** The mole fraction of FeS in sphalerite, X_{FeS}, reflects temperature and activity of sulfur conditions during ore deposition (Scott and Barnes, 1971).

Sphalerite from Kam Group samples has X_{FeS} values of 0.12 to 0.27. Samples from Banting Group localities have X_{FeS} values of 0.09 to 0.24. No systematic compositional zoning in sphalerite grains was observed.

The range of X_{FeS} values for sphalerite is consistent with sphalerite that is in equilibrium with pyrite (lower X_{FeS} values) or pyrrhotite (higher X_{FeS} values). Pyrite and pyrrhotite were both observed to be intergrown with sphalerite in the Kam and Banting Groups. If sphalerite were precipitated at the same high temperatures as early mineralization (350° to 400°C), its X_{FeS} values would reflect log activity of sulfur values near -7. If sphalerite formed at lower temperatures (~250°C), its X_{FeS} values would reflect log activity of sulfur values near -12. In either case, during sphalerite deposition, ore fluids were close to equilibrium with pyrite and pyrrhotite. Small changes in temperature and/or activity of sulfur would result in the observed X_{FeS} contents of all of the sphalerites.

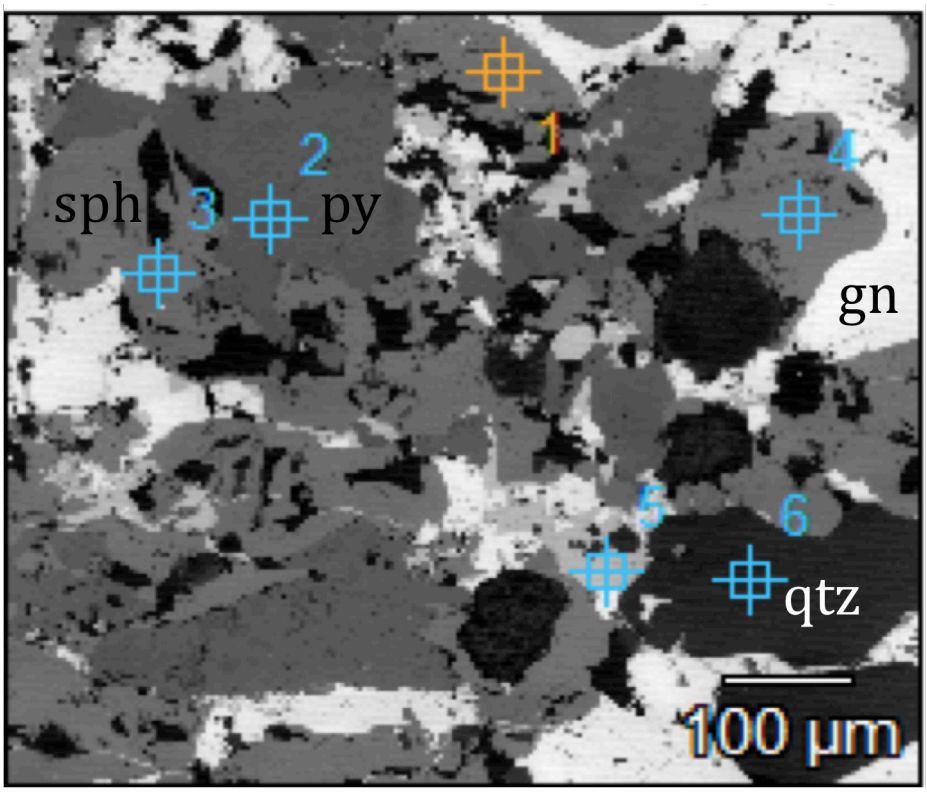

Figure 21. Backscatter electron image of sphalerite intergrown with pyrite from Homer Lake (Kam Group). Crosshairs show locations of spot analysis.

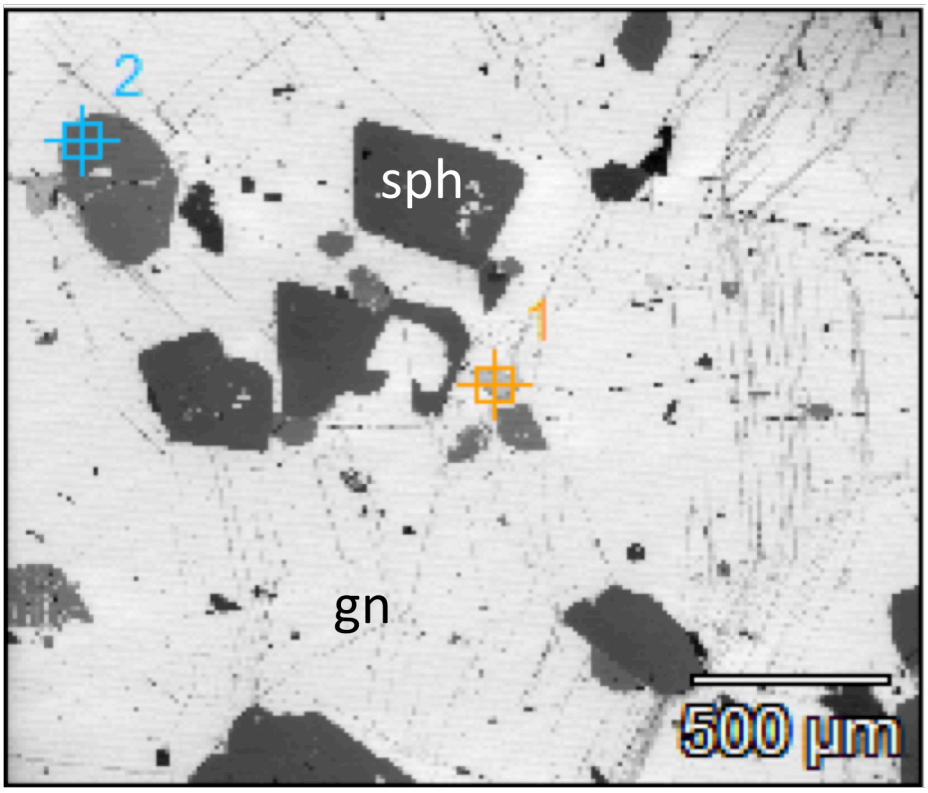

Figure 22. Backscatter electron image of sphalerite crystals in galena from Homer Lake (Kam Group).

Arsenopyrite

SEM study revealed zoning in arsenopyrite from the Ann claims at Walsh Lake (Banting Group; Fig. 23). Backscatter images of the arsenopyrite show the cores of some crystals to be dark, with lighter rims. Compositional analysis reveals that, from core to rim, sulfur content decreases (35.7 mole % to 32.0 mole %), arsenic content increases (29.2 mole % to 32.1 mole %), and iron content increases (35.1 mole % to 35.9 mole %).

Compositional zoning in arsenopyrite was not observed in any other samples. Compositions of arsenopyrite from Kam Group samples are remarkably uniform, with the average sulfur content near 32.7 mole %, average arsenic content near 32.8 mole % and average iron content near 34.5 mole %. These values are similar to values measured for arsenopyrite rims from the Ann claims of the Banting Group.

The presence of multiple generations of arsenopyrite at the Ann claims (Banting Group) and compositional zonation indicates that either multiple fluids were responsible for precipitation of arsenopyrite, or that temperature and/or fluid composition changed over time (for a description of the use of arsenopyrite as a geothermometer, see Sharp et al., 1985).

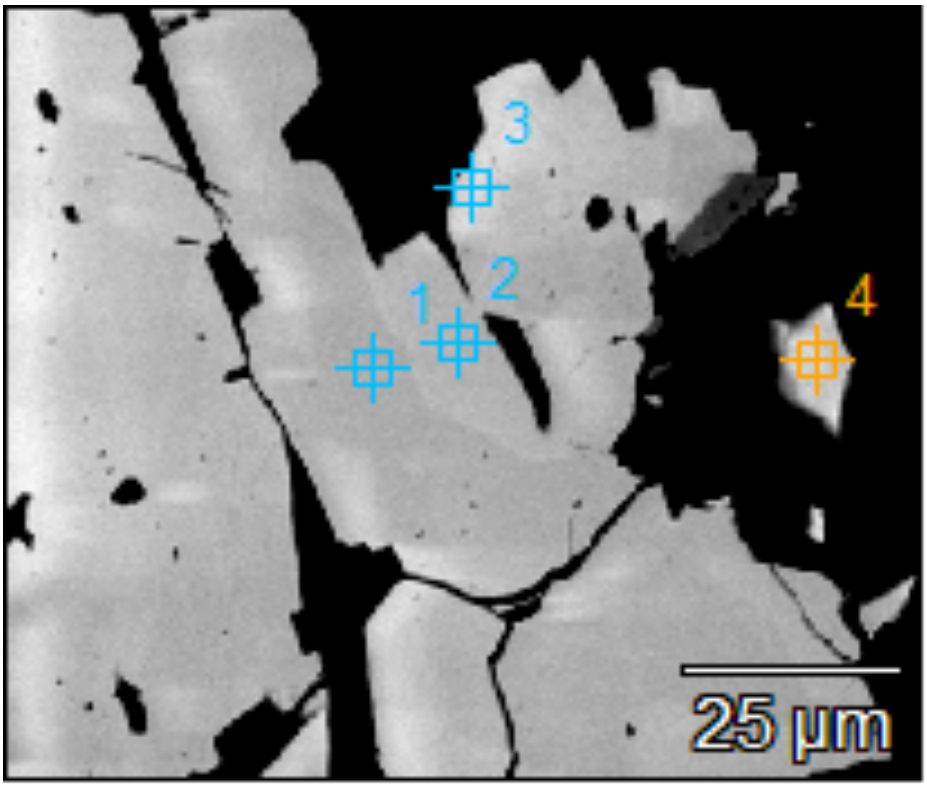

Figure 23. SEM backscatter image of zoned arsenopyrite from the Ann claims (Banting Group). Numbered spots indicate locations for spot analysis of arsenopyrite compositions. Note darker cores and lighter rims. Darker areas are more sulfur-rich, whereas lighter areas area more Fe- and As- rich.

Gold

Using SEM, two generations of gold were documented in the Banting Group. The first generation occurs as discrete (<3 μm) inclusions within arsenopyrite (Fig. 24). Compositional analysis of early generation gold reveals X_{Ag} (molar) values of ~0.2 to 0.3. The later generation of gold was observed as isolated blebs occurring in veins and in altered wall rock or occurring along fractures and veinlets in sulfides (Fig. 24 & 25). This later generation of gold is more silver-rich, with X_{Ag} values up 0.5.

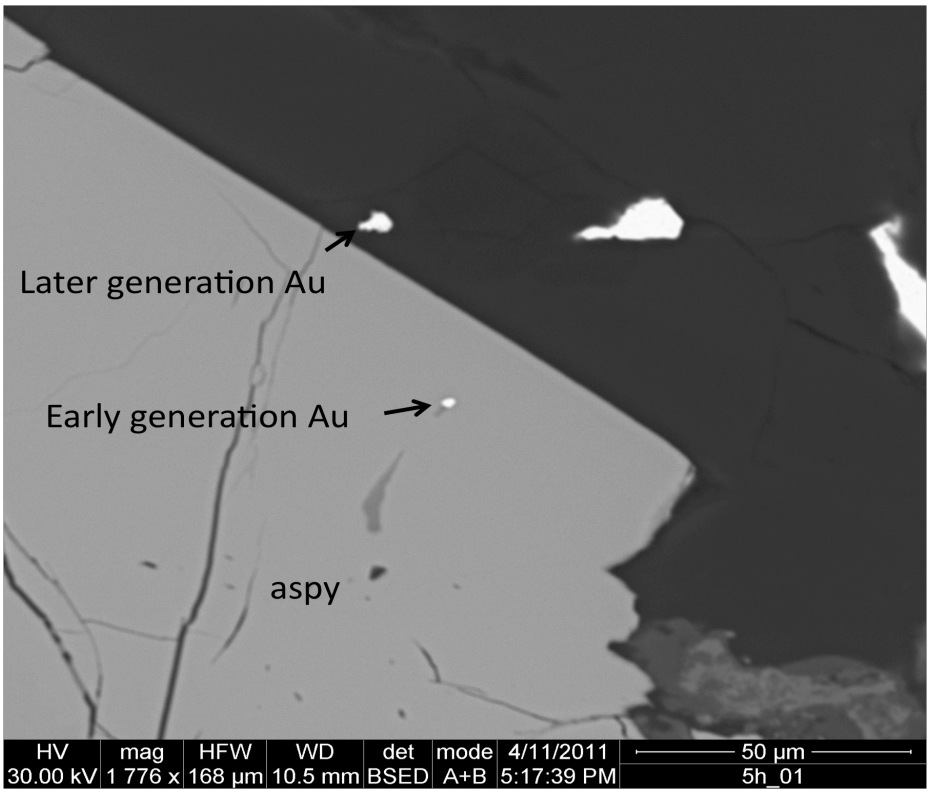

Figure 24. SEM backscatter image shows two generations of gold in the Ann claims (Banting Group). Early gold (X_{Ag} ~0.3) is hosted as discrete inclusions within arsenopyrite (aspy). The later generation (X_{Ag} ~0.4 to 0.5) is frequently found as isolated blebs in quartz or altered wall rock, or infilling fractures in earlier sulfides.

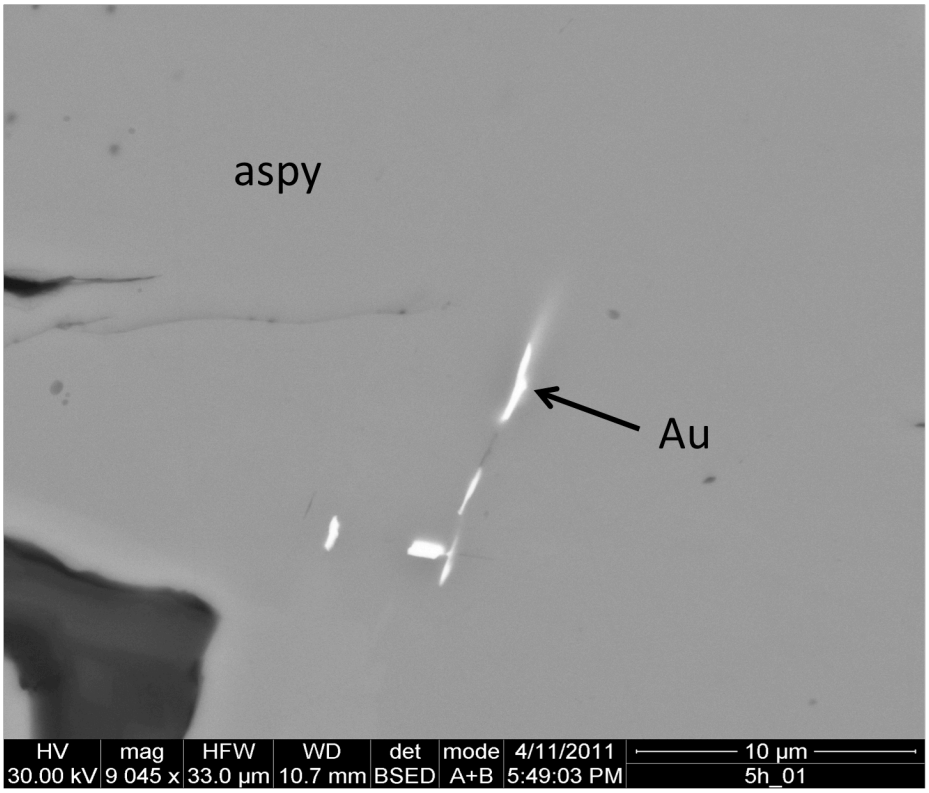

Figure 25. Later gold (Au) infilling a fracture and replacing arsenopyrite (aspy) in a quartz vein from the Ann claims (Banting Group).

Odd Phases

Several distinct phases were observed under reflected light microscopy, and SEM was employed to determine compositions of unknown phases. Of particular note, in a sample from Samex Island (Banting Group) we observed native bismuth occurring with galena (Fig. 26). Other rare phases that were found include silver tellurides and sulfosalts.

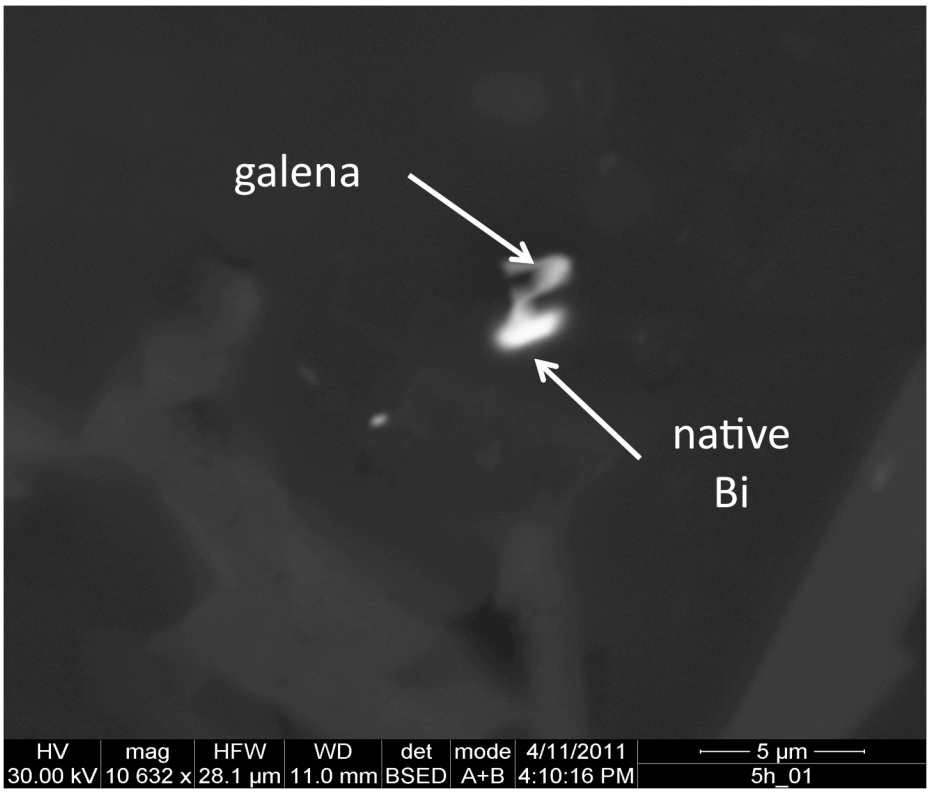

Figure 26. Native bismuth (bright bleb) and galena within altered wall rock from Samex Island (Banting Group).

CHAPTER VII: CONCLUSIONS

The thermal, chemical and fluid evolution of gold and base-metal sulfide mineralization in the Kam and Banting Groups of the north end of the YGB were determined by ore, CL, and SEM microscopy, fluid inclusion microthermometry, and oxygen isotope geochemistry. Conclusions that can be reached, based on mineralized areas studied are:

(1) The varieties of ore mineralization styles within the Chan Formation of the Kam Group formed at different relative ages over an extended period of geologic time (from > 2738 Ma to < 2608 Ma). Though there is a similarity in typical ore mineralogy and paragenesis (early arsenopyrite-pyrite-gold overprinted by late base-metal sulfides), the mineralized areas are likely the products of distinct hydrothermal systems.

(2) Mineralization in showings in the Banting Group is dominated by abundant pyrrhotite, a feature not observed by us in the Chan Formation (Kam Group). This may indicate that chemically unique ore-depositing systems operated within the Banting Group. Two generations of gold are present in Banting Group samples; the early generation is hosted as inclusions in sulfides and the later generation occurs in wall rock and quartz veins that crosscut and replace sulfides.

(3) Dolomite-ankerite (post gold-ore) in quartz veins of the Chan Formation (Kam Group) exhibits similar cathodoluminescence zoning (CL) in mineral showings up to 5 km apart. Similar CL zoning is not observed in

carbonates in the Banting Group, indicating a lack of fluid communication between the Kam and Banting Groups at that time.

(4) Paragenetically later calcite exhibits similar CL patterns in the Kam and Banting Groups, likely indicating that both groups were affected by common hydrothermal systems during the time of late calcite deposition.

(5) Post-ore, aqueous brine and halite-bearing fluid inclusions are ubiquitous in the Kam and Banting Groups and indicate pervasive fluid movement through both groups. These late brines are similar to those observed in many areas of the Slave Province that have been affected by Proterozoic fault systems.

(6) Oxygen isotope compositions of quartz veins and calculated water values indicate the influence of two distinct types of fluid reservoirs (metavolcanic and metasedimentary) during ore deposition. Large deposits in the Yellowknife area are in part the result of interplay of fluids from both types of reservoirs. Lack of communication/overlap of metasedimentary and metavolcanic fluid reservoirs may explain why no large deposits have been found in our study area. We speculate that faults that define the contacts between the Kam and Banting Groups are steeply dipping and did not allow fluid communication during ore-deposition.

(7) Implications for future exploration: Application of geochemical techniques to other areas in the YGB may allow us to test the influence of metasedimentary and metavolcanic fluids. For example, at Ormsby Lake, a smaller (200 m x 1 km) lens of mafic metavolcanic rock occurring with a much

larger volume of metasedimentary rocks contains ~1.2 million troy ounces of measured and inferred gold (Pratico, 2009). This is the ideal setting to evaluate the influence of multiple fluid reservoirs of the development of economic gold deposits in the YGB.

REFERENCES

Armstrong, J.P., 1997, Variations in silicate and sulfide mineral chemistry between free-milling “metallic” and refractory “invisible” gold ores, Con mine, Yellowknife, N.W.T.: Unpublished Ph.D. dissertation, London, ON, University of Western Ontario, 239 pp.

Bakker, R.J., and Jansen, B.H., 1990, Preferential water leakage from fluid inclusions by means of mobile dislocation; Nature, v. 345, p. 58-60.

Bethune, K.M., Villeneuve, M.E., Bleeker, W., 1999, Laser $^{40}Ar/^{39}Ar$ thermochronology of Archean rocks in Yellowknife Domain, southwestern Slave Province: insights into the cooling history of an Archean granite-greenstone terrane. Canadian Journal of Earth Sciences, v. 36, p. 1189-1206.

Bleeker, W., and Hall, B., 2007, The Slave Craton: Geology and metallogenic evolution. *in* Goodfellow, W.D., ed., Mineral Deposits of Canada: A Synthesis of Major Deposit-Types, District Metallogeny, the Evolution of Geological Provinces, and Exploration Methods; Geological Association of Canada, Mineral Deposits Division, Special Publication 5, p. 849-879.

Bleeker, 2002, Archean tectonics: a review, with illutrations from the Slave craton. *in* Fowler, C.M.R., Ebinger, C.J., and Hawkseworth, C.J., eds., The Early Earth: Physical, Chemical and Biological Development, Geological Society Special Publications No. 199, p. 151-181.

Bodnar, R.J., and Vityk, M.O., 1994, Interpretation of microthermometric data for H_2O-NaCl fluid inclusions. *in* De Vino, B., and Frezzotti, M.L., eds., Fluid Inclusions in Minerals: Methods and Applications; Virginia Polytechnic Institute and State University, p. 11-130.

Brown, P.E., and Hagemann, S.G., 1995, MacFlinCor and its application to fluids in Archean lode-gold deposits; Geochimica et Cosmochimica Acta, v. 19, p. 3943-3952.

Bullen, W., and Robb, M., 2006, Socio-economic impacts of mining in the Yellowknife mining district, *in* Anglin, C.D., Falck, H., Wright, D.F., and Ambrose, E.J., eds., Gold in the Yellowknife Greenstone Belt, Northwest Territories: Results of the EXTECH III Multidisciplinary Research Project; Geological Association of Canada, Mineral Deposits Division, Special Publication 3, p. 38-48.

Costello, C.S., 1999, Geochemical and fluid inclusion studies of the Colomac mine, NWT, Canada: Unpublished M.S. thesis, University of Missouri, Columbia, 129 pp.

Craw, D., and Norris, R.J., 1993, Grain boundary migration of water and carbon dioxide during uplift of garnet-zone Alpine schist, New Zealand; Journal of Metamorphic Geology, v. 11, p. 371-378.

Davis, W.J., Bleeker, W., Hulbert, L., and Jackson, V., 2004, New geochronological results from the Slave Province Minerals and Geoscience Compilation and Synthesis Project, GSC Northern Resources Program; 37th Annual Yellowknife Geoscience Forum, p. 20.

Davis, W.J., and Bleeker, W., 1999, Timing of plutonism, deformation, and metamorphism in the Yellowknife Domain, Slave Province, Canada. Canadian Journal of Earth Sciences, v. 36, p. 1169-1187.

Davis, W. J., Jones, A.G., Bleeker, W., and Grütter, H., 2003, Lithosphere development in the Slave craton: a linked crustal and mantle perspective. Lithos, v. 71, p. 575-589.

English, P.J., 1981, Gold-quartz veins in metasediments of the Yellowknife Supergroup, Northwest Territories: A fluid inclusion study; Unpublished M.Sc. thesis, University of Alberta, 108 pp.

Götze, J., Plötze, M., and Habermann, D., 2001, Origin, spectral characteristics and practical applications of the cathodoluminescence (CL) of quartz: a review. Mineralogy and Petrology, v. 71, p. 225−250.

Ho, S.E., Groves, D.I., McNaughton, N.J., and Mikucki, E.J., 1992, The source of ore fluids and solutes in Archean lode-gold deposits of Western Australia; Journal of Volcanology and Geothermal Research, v. 50, p. 173-196.

Hill, L., 2010, Ore petrology of gold and base-metal mineralization in the north end of the Yellowknife greenstone belt, NWT, Canada: Unpublished B.S. thesis, University of Missouri, Columbia, 55 pp.

Hollister, L.S., 1990, Enrichment of CO_2 in fluid inclusions in quartz by removal of H_2O during crystal-plastic deformation; Journal of Structural Geology, v. 12, p. 895-901.

Isachsen, C.E., Bowring, S.A., 1997, The Bell Lake Group and Anton Complex. a basement-cover sequence beneath the Archean Yellowknife greenstone belt revealed and implicated in greenstone belt formation. Canadian Journal of Earth Sciences, v. 34, p. 169-189.

Johnson, E.L., and Hollister, L.S., 1995, Syndeformational fluid trapping in quartz: Determining the pressure-temperature conditions of deformation from fluid inclusions and the formation of pure CO_2 fluid inclusions during

grain boundary migration; Journal of Metamorphic Geology, v. 13, p. 239-249.

Kerrich, R., and Fyfe, W.S., 1981, The gold-carbonate association: Source of CO_2 and CO_2-fixation reactions in Archean lode gold deposits; Chemical Geology, v. 33, p. 265-294.

Kerrick, D.M., and Jacobs, G.K., 1981, A modified Redlich-Kwong equation of H_2O, CO_2, and H_2O-CO_2 mixtures at elevated pressures and temperatures; American Journal of Science, v. 281, p. 735-767.

Kerswill, J.A., and Falck, H., 2002, Regional metallogeny of the Yellowknife EXTECH area, Northwest Territories, Canada; Geological Association of Canada-Mineralogical Association of Canada Annual Meeting, Program and Abstracts, v. 27, p. 59-60.

Kusky, T.M., 1989, Accretion of the Archean Slave Province. Geology, v. 17, p. 63-67.

Landtwing, M.R. and Pettke, T., 2005, Relationships between SEM-cathodoluminescence response and trace-element composition of hydrothermal vein quartz. American Mineralogist, v. 90, p. 122–131.

MacLachlan, K., and Davis, W.J., 2002, Uranium-lead ages of Defeat granitoid rocks near the Con mine, Northwest Territories: Geological Survey of Canada Current Research 2002-F1, 9 pp.

Marshall, B., and Gilligan, L., 1989, Durchbewegung structure, piercement cusps, and piercement veins in massive sulfide deposits: formation and interpretation; Economic Geology, v. 84, p. 2311-2319.

Martel, E., and Lin, S., 2006, Structural evolution of the Yellowknife greenstone belt, with emphasis on the Yellowknife River Fault Zone and the Jackson Lake Formation, *in* Anglin, C.D., Falck, H., Wright, D.F., and Ambrose, E.J., eds., Gold in the Yellowknife Greenstone Belt, Northwest Territories: Results of the EXTECH III Multidisciplinary Research Project; Geological Association of Canada, Mineral Deposits Division, Special Publication 3, p. 95-115.

Muller, A., Lennox, P., and Trzebski, R., 2002, Cathodoluminescence and microstructural evidence for crystallization and deformation processes of granites in the Eastern Lachlan Fold Belt (SE Australia). Contributions to Mineralogy and Petrology, v. 143, p. 510–524.

Ootes, L., Morelli, R.M., Lentx, D.R., Falck, H., Creaser, R.A., and Davis, W.J., *in press,* The timing of Yellowknife gold mineralization: a temporal relationship with crustal anatexis?; Economic Geology.

Ootes, L., Buse, S., Davis, W.J., and Cousens, B., 2005, U-Pb Ages from the Northern Wecho River Area, Southwestern Slave Province, Northwest Territories: Constraints on Late Archean Plutonism and Metamorphism: Geological Survey of Canada, Current Research 2005-F2, 13 pp.

Practico, V., 2009, Report on the Resource Estimate of the Yellowknife Gold Project; Tyhee Development Corporation, Vancouver, BC, Canada, 79 pp.

Relf, C., 1988, The alteration history of a series of shear zones, Mirage Islands, Yellowknife Bay, N.W.T.; Unpublished M.Sc. thesis, Memorial University of Newfoundland, 125 pp.

Ripple, A., Shelton, K.L., and Falck, H., 2009, Fluid and thermal history of a breccia zone of the West Bay Fault, NWT; 37th Annual Yellowknife Geoscience Forum, p. 88.

Samson, I.M., Bulent, B., and Holm, P.E., 1997, Hydrothermal evolution of auriferous shear zones, Wawa, Ontario; Economic Geology, v. 92, p. 325-342.

Scott, S., and Barnes, H.L., 1971, Sphalerite geothermometry and geobarometry; Economic Geology, v. 66, 653-669.

Sharp, Z.D., Essene, E.J., and Kelly, W.C., 1985, A re-examination of the arsenopyrite geothermometer: pressure considerations and applications to natural assemblages; Canadian Mineralogist, v. 23, p. 517-534.

Shelton, K.L., Costello, C.S., and van Hees, E.H., 2000, Contrasting styles of Archean greenstone gold deposition: Colomac gold mine, Canadian Northwest Territories; Journal of Geochemical Exploration, v. 69-70, p. 303-307.

Shelton, K.L., McMenamy, T.A., van Hees, E.H.P., and Falck, H., 2004, Deciphering the complex fluid history of a greenstone-hosted gold deposit: Fluid inclusion and stable isotope studies of the Giant mine, Northwest Territories, Canada; Economic Geology, v. 99, p. 1643-1663.

Siddorn, J.P., Cruden, S., Armstrong, J., Hubbard, L., 2006, The Giant-Con deposits: Structural and mineralization history, *in* Anglin, C.D., Falck, H., Wright, D.F., and Ambrose, E.J., eds., Gold in the Yellowknife Greenstone Belt, Northwest Territories: Results of the EXTECH III multidisciplinary research project; Geological Association of Canada, Mineral Deposits Division, Special Publication 3, p. 213-231.

Thiery, R., van den Kerkhof, A.M., and Dubessy, J., 1994, vX properties modeling of CH_4-CO_2 and CO_2-N_2 fluid inclusions (T < 31˚C, P < 400 bars); European Journal of Mineralogy, v. 6, p. 753-771.

Thompson, P.H., 2006, Chapter 11: Metamorphic constraints on the geological setting, thermal regime, and timing of alteration and gold mineralization in the Yellowknife Greenstone Belt, NWT, Canada: Geological Association of Canada Mineral Deposits Division Special Publication no. 3, p. 142–172.

van Breemen, O., Davis, W.J., and King, J.E., 1992, Temporal distribution of granitoid plutonic rocks in the Archean Slave Province, northwestern Canadian Shield; Canadian Journal of Earth Sciences, v. 29, p. 2186-2199.

van Hees, E H., Kirkham, G.D., Sirbescu, M-L., Shelton, K.L., Hauser, R., and Falck, H., 2006, Large lithogeochemical alteration halos around Yellowknife gold deposits and implications for fluid pathways. *in* Anglin, C.D., Falck, H., Wright, D.F., and Ambrose, E.J., eds., Gold in the Yellowknife Greenstone Belt, Northwest Territories: Results of the EXTECH III multidisciplinary research project; Geological Association of Canada, Mineral Deposits Division, Special Publication 3, p. 232-248.

van Hees, E.H.P., Shelton, K.L., McMenamy, T.A., Ross, L.M. Jr., Cousens, B.L., Falck, H., Robb, M.E., and Canam, T.W., 1999, Metasedimentary influence on metavolcanic-rock-hosted greenstone gold deposits: Geochemistry of the Giant mine, Yellowknife, Northwest Territories, Canada; Geology, v. 27, p. 71-74.

Zhang, Y.G., and Frantz, J.D., 1989, Experimental determination of the compositional limits of immiscibility in the system $CaCl_2$-H_2O-CO_2 at high temperatures and pressures using synthetic fluid inclusions; Chemical Geology, v. 74, p. 289-308.

APPENDIX:

I. Sample Descriptions

Kam Group

Sample	Location UTM	Description
AL-09-1	637136E, 6950129N	quartz vein with large arsenopyrite xtll
AL-09-2	637136E, 6950129N	massive arsenopyrite
AL-09-3	637136E, 6950129N	arsenopyrite with quartz
AL-09-4	637136E, 6950129N	coarse aspy
AL-09-5	637158E, 6950179N	coarse-grained arsenopyrite
AL-09-6	637158E, 6950179N	sheared zone with fluorite
AL-09-7	637158E, 6950179N	sheared wall rock with sulfides
BC-09-1	639532E, 6953263N	quartz vein (several cm wide) with minor sulfides in altered mafic rocks (Basal Kam)
BC-09-2	637502E, 6953538N	massive sulfide
BC-09-3	637506E, 6953580N	quartz + arsenopyrite
BC-09-4	637506E, 6953580N	cm-scale euhedral quartz crystals in vuggy portions of vein
BC-09-5	637381E, 6952794N	quartz vein with copper staining
BC-09-6	637381E, 6952794N	quartz vein in wall rock with orange-pink mineral
CL-09-1	635679E, 6948097N	pink quartz vein
CL-09-2	635679E, 6948097N	quartz + arsenopyrite
CL-09-3	636775E, 6948177N	quartz vein with copper alteration
CL-09-4	635679E, 6948097N	quartz + chalcopyrite ± bornite
GL-09-1A	638245E, 6953705N	barren quartz
GL-09-1B	638245E, 6953705N	euhedral barren quartz
GL-09-2A	638064E, 6952719N	quartz plus minor sulfides
GL-09-2B	638064E, 6952719N	carbonate in same vein
GL-09-3	638059E, 6952609N	quartz vein with sulfides
GL-09-4	638059E, 6952609N	massive coarse-grained arsenopyrite with quartz
GL-09-5	638059E, 6952609N	quartz vein with chalcopyrite
GL-09-6	638059E, 6952609N	actinolite growing into sulfides
GL-09-7	638059E, 6952609N	fine-grained arsenopyrite
GL-09-8	638059E, 6952609N	skarnish alteration (w/sulfides) for thin-section
GL-09-9	638059E, 6952609N	large skarn alteration sample w/ actinolite spray (do not cut)
GL-09-10	638059E, 6952609N	thin zone of red-altering pyrite
GL-09-11	638059E, 6952609N	granular weathered sphalerite
HL-09-1	638345E, 6950163N	Massive arsenopyrite, minor galena ±pyrite
HL-09-1A	638345E, 6950163N	massive arsenopyrite with quartz
HL-09-1B	638345E, 6950163N	massive arsenopyrite + other sulfides (more quartz than usual)

HL-09-2	638345E, 6950163N	quartz vein on SE side of trench (only) semi-parallel to sulfide zone bearing some pyrite. Late vuggy quartz with chalcopyrite.
HL-09-3	638345E, 6950163N	massive galena ±sphalerite
HL-09-4	638329E, 6950099N	massive arsenopyrite±pyrite
HL-09-5	638329E, 6950099N	massive galena + sphalerite
HL-09-6	638329E, 6950099N	massive arsenopyrite + chalcopyrite
HL-09-7	638357E, 6950127N	massive arsenopyrite + quartz
HL-09-8A	638313E, 6949791N	coarse-grained galena
HL-09-8B	638313E, 6949791N	massive arsenopyrite + quartz
HL-09-9	638313E, 6949791N	quartz vein not associated with sulfides for CL comparison
HL-09-10A	638110E, 6950279N	quartz vein with arsenopyrite
HL-09-10B	638110E, 6950279N	barren quartz
HL-09-10C	638110E, 6950279N	massive arsenopyrite
HL-09-10D	638110E, 6950279N	arsenopyrite in quartz at shear intersection
HL-09-11A	638377E, 6949942N	durchbewegen quartz clots in massive sulfide (quartz veins milled to rounded fragments floating in sulfide)
HL-09-11B	638377E, 6949942N	quartz vein with galena + black jack sphalerite ± chalcopyrite?
HL-09-12	637689E, 6950565N	molybdenite in aplitic dike with quartz veins
HL-09-13	637689E, 6950565N	magnetite alteration in metabasalt near igneous contacts
HL-09-14	638345E, 6950163N	host rock in shear of main trench. Altered felsic rock w/ quartz eyes. Contains sulfides (aspy?)
HL-09-15	638349E, 6949701N	quartz with sulfides
HL-09-16	638377E, 6949942N	arsenopyrite
HL-09-17	638377E, 6949942N	quartz + chalcopyrite
HL-09-18	638227E, 6950011N	massive arsenopyrite
HL-09-19	638227E, 6950011N	massive arsenopyrite
HL-09-20	638227E, 6950011N	massive and coarse-grained arsenopyrite
OL-09-1A	636645E, 6948067N	quartz vein
OL-09-1B	636645E, 6948067N	quartz vein ± sulfides
OL-09-2	636645E, 6948067N	quartz + chalcopyrite + other sulfides
Ol-09-3	636645E, 6948067N	quartz vein ± sulfides
Ol-09-4	636472E, 6948108N	barren quartz for comparison
OL-09-5	636645E, 6948067N	massive sulfide

Banting Group

Sample	Location UTM	Description
BL-09-1	640161E, 6946860N	complete quartz vein (2 cm)
BL-09-2	640161E, 6946860N	quartz vein with yellow-brown glassy mineral
BL-09-3	640161E, 6946860N	quartz vein with orange mineral (feldspar?)
BL-09-4	640069E, 6947969N	blue quartz vein
BL-09-5	640069E, 6947969N	biotite-rich? Host rock
BL-09-6	640024E, 6948172N	arsenopyrite-rich zone in wall rock
BL-09-7	640024E, 6948172N	arsenopyrite-rich zone in wall rock
BL-09-8	640024E, 6948172N	arsenopyrite-rich zone in wall rock
BL-09-9	640024E, 6948172N	quartz veins in wall rock with arsenopyrite ± cpy?
BL-09-10	638949E, 6944315N	quartz ± minor carbonate vein in sheared wallrock with minor sulfides
SI-09-1	639590E, 6948773N	blue quartz + muscovite + arsenopyrite crystals
SI-09-2	639590E, 6948773N	clean blue quartz w/o other minerals
SI-09-3	639590E, 6948773N	massive sulfide with arsenopyrite
SI-09-4	639590E, 6948773N	host rock (sericitized?)
SI-09-5	632649E, 6949194N	blue quartz vein with arsenopyrite and bornite?
SI-09-6	632649E, 6949194N	blue quartz with muscovite
WL-09-1	640250E, 6945838N	quartz with arsenopyrite in wall-rock stringers
WL-09-2	640250E, 6945838N	host rock with arsenopyrite
WL-09-3	640955E, 6942455N	quartz vein with arsenopyrite
WL-09- 4	640955E, 6942455N	felsic rock immediately west of arsenopyrite-rich host rock.
WL-09-5A	640955E, 6942455N	arsenopyrite-rich host rock
WL-09-5B	640955E, 6942455N	arsenopyrite-rich host rock
WL-09-5C	640955E, 6942455N	arsenopyrite-rich host rock
WL-09-6	640955E, 6942455N	arsenopyrite-rich host rock with visible sprays of amphibole
WL-09-7	640955E, 6942455N	large aspy in wall rock
WL-09-8	639751E, 6944416N	quartz vein with arsenopyrite
WL-09-9	639751E, 6944416N	sulfides in wall rock with quartz
WL-09-10	639751E, 6944416N	quartz vein with sulfides
WL-09-11	640907E, 6942347N	arsenopyrite adjacent to quartz vein
WL-09-12	640907E, 6942347N	massive arsenopyrite
WL-09-13	640907E, 6942347N	coarse-grained sphalerite on quartz
WL-09-14	640907E, 6942347N	fine-grained sphalerite
WL-09-15	640907E, 6942347N	fine-grained sphalerite with quartz
WL-09-16	640907E, 6942347N	coarse-grained sphalerite
WL-09-17	640907E, 6942347N	fine-grained sphalerite + galena
WL-09-18	640051E, 6944271N	massive arsenopyrite (2 pieces)
WL-09-19	640051E, 6944271N	gray quartz with minor sulfides

Sample	Inclusion #	$T_{f\ CO2}$ (°C)	$T_{m\ CO2}$ (°C)	$T_{h\ CO2}$ (°C)	$T_{m\ clath}$ (°C)	T_h (°C)	CO_2 area %	Homogenized or Decrepitated	Density (g/cm^3) carbonic	Density (g/cm^3) total	XCH_4 carbonic	XCH_4 total	Salinity (wt% equiv. NaCl)
AL-09-1	1	-97.5	-57.5	29.3	1.0	367.0	50.0	homogenized	0.49	0.80	0.05	0.01	14.41
AL-09-1	2	-97.1	-56.5	26.1	-14.0	-	100.0	n/a	0.69	0.69	0.00	0.00	21.43
AL-09-1	3	-100.0	-56.5	27.9	22.9	-	100.0	n/a	0.66	0.66	0.00	0.00	0.02
AL-09-1	4	-96.4	-56.5	19.8	-42.8	-	100.0	n/a	0.78	0.78	0.00	0.00	21.43
AL-09-3	1	-96.8	-57.0	25.9	-10.6	341.6	50.0	decrepitated	0.49	0.83	0.05	0.83	21.43
AL-09-6	1	-86.7	-56.5	27.7	-10.2	384.0	50.0	homogenized	0.66	0.91	0.00	0.00	21.43
AL-09-6	2	-89.5	-56.5	28.6	-10.2	364.0	80.0	decrepitated	0.64	0.74	0.00	0.00	21.43
AL-09-6	3	-95.5	-56.5	29.9	6.7	-	100.0	n/a	0.60	0.60	0.00	0.00	6.20
AL-09-6	4	-95.6	-56.5	31.1	6.7	-	100.0	n/a	0.53	0.53	0.00	0.00	6.20
AL-09-6	5	-95.6	-56.5	29.9	6.7	-	100.0	n/a	0.60	0.60	0.00	0.00	6.20
AL-09-6	6	-95.6	-56.5	29.9	6.7	-	100.0	n/a	0.60	0.60	0.00	0.00	6.20
AL-09-7	1	-97.9	-58.5	22.6	2.4	449.0	20.0	n/a	0.49	0.97	0.05	0.00	12.68
AL-09-7	2	-95.1	-56.5	31.2	5.7	350.0	50.0	homogenized	0.53	0.79	0.00	0.00	7.87
AL-09-7	3	-95.1	-56.5	31.2	6.4	339.1	40.0	homogenized	0.53	0.84	0.00	0.00	6.71
AL-09-7	4	-93.5	-56.5	23.4	-6.3	-	100.0	n/a	0.73	0.73	0.00	0.00	20.37
AL-09-7	5	-93.7	-56.5	26.0	-8.7	-	100.0	n/a	0.70	0.70	0.00	0.00	21.21
AL-09-7	6	-66.9	-56.5	23.5	17.9	-	100.0	n/a	0.73	0.73	0.00	0.00	0.02
AL-09-7	7	-68.7	-56.5	23.5	10.4	-	100.0	n/a	0.73	0.73	0.00	0.00	0.02
AL-09-7	8	-69.9	-56.5	23.7	16.0	-	100.0	n/a	0.73	0.73	0.00	0.00	0.02
AL-09-7	9	-69.0	-56.7	25.3	-4.4	-	100.0	n/a	0.49	0.50	0.05	0.05	19.31
AL-09-7	10	-96.2	-56.7	25.3	-4.4	-	100.0	n/a	0.49	0.50	0.05	0.05	19.31
OL-09-4	1	-100.0	-59.0	24.6	-5.7	330.0	50.0	homogenized	0.49	0.82	0.05	0.01	20.07
OL-09-4	2	-100.0	-57.3	23.2	-5.7	316.0	50.0	decrepitated	0.49	0.82	0.05	0.01	20.07
OL-09-4	3	-78.9	-57.2	22.9	5.7	334.6	50.0	homogenized	0.49	0.78	0.05	0.01	7.87
OL-09-4	4	-89.5	-59.7	23.5	0.1	335.1	50.0	homogenized	0.49	0.81	0.05	0.01	15.42
OL-09-4	5	-80.7	-58.3	15.4	-18.8	-	100.0	n/a	0.49	0.50	0.05	0.05	21.43
GL-09-3	1	-95.2	-56.6	22.7	-	-	100.0	n/a	-		0.00	0.00	-
GL-09-3	2	-94.2	-56.6	24.6	-	-	100.0	n/a	-		0.00	0.00	-
GL-09-3	3	-77.2	-56.6	19.6	-	-	100.0	n/a	-		0.00	0.00	-
GL-09-3	4	-83.5	-56.8	27.6	-	-	100.0	n/a	-		0.00	0.00	-
GL-09-3	5	-77.2	-56.9	24.3	-	-	100.0	n/a	-		0.00	0.00	-
HL-09-2	1	-97.1	-57.4	27.1	-2.5	-	50.0	n/a	0.49	0.82	0.05	0.01	17.90
HL-09-2	2	-97.1	-56.8	25.2	-10.5	-	50.0	n/a	0.49	0.83	0.05	0.01	21.43
HL-09-2	3	-94.4	-56.8	28.5	22.6	-	50.0	n/a	0.49	0.75	0.05	0.01	0.02

Sample	Inclusion #	$T_{f\ CO2}$ (°C)	$T_{m\ CO2}$ (°C)	$T_{h\ CO2}$ (°C)	$T_{m\ clath}$ (°C)	T_h (°C)	CO2 area %	Homogenization (h) or Decrepitated (d)	Density (g/cm3) carbonic	density total	XCH4 carbonic	XCH4 total	Salinity (wt% equiv. NaCl)
HL-09-2	5	-88.7	-56.7	19.5	-3.3	-	50.0	n/a	0.49	0.82	0.05	0.01	18.54
HL-09-2	6	-98.0	-57.8	23.5	-12.5	-	50.0	n/a	0.49	0.83	0.05	0.01	21.43
HL-09-2	7	-94.3	-56.7	16.1	-3.3	-	50.0	n/a	0.49	0.82	0.05	0.01	18.54
HL-09-2	8	-89.2	-57.1	29.1	-17.9	322.2	90.0	homogenized	0.49	0.57	0.05	0.03	21.43
HL-09-2	9	-92.8	-57.8	28.3	-9.9	393.5	90.0	homogenized	0.49	0.57	0.05	0.03	21.42
HL-09-2	10	-95.0	-56.6	29.2	-5.5	357.1	50.0	homogenized	0.63	0.88	0.00	0.00	19.96

III. Oxygen Isotopes

KAM GROUP

SAMPLE	DESCRIPTION	$\delta^{18}O$(‰) V-SMOW
AL-09-7	large qtz grains with undulose extinction	8.3
BC-09-4	late euhedral quartz	12.6
BC-09-4 DUP	DUPLICATE	12.4
CL-09-1	pink qtz vein	11.0
GL-09-1B	late euhedral barren quartz, large euhedral grains of qtz with sharp boundaries and no deformation	10.0
GL-09-5	qtz vein with chalcopyrite	11.2
GL-09-8	skarnish alteration with sulfides	10.4
HL-09-2	late vuggy quartz	11.6
HL-09-2 DUP	DUPLICATE	11.6
HL-09-9	qtz vein not associated with sulfides	11.3
HL-09-10A	larger qtz present w/ undulose extinction	11.8
HL-09-10B	barren qtz	11.4
HL-09-10D	highly sheared qtz; curvy grain boundaries within qtz	11.1
HL-09-15	highly sheared qtz; main stage	10.8
HL-09-17	highly sheared qtz with late euhedral qtz	11.4
OL-09-3	high recovery	10.6
OL-09-4	late barren qtz	10.2

BANTING GROUP

SAMPLE	DESCRIPTION	δ18O(‰) V-SMOW
BL-09-1	complete quartz vein	14.4
BL-09-4	blue qtz vein	14.8
SI-09-2	clean blue qtz w/o other minerals	14.6
WL-09-3	qtz vein with arsenopyrite	14.7
WL-09-19	gray qtz with minor sulfides	13.2
WL-09-19 DUP	DUPLICATE	13.4